

Quantum Monte Carlo Study of the Bilinear Biquadratic Spin-1 Model



A Thesis Submitted for the Degree of
Master of Science
Ludwig-Maximilians-Universität München

Julian Durnwalder

Advisor: Prof. Dr. Lode Pollet

München, January 21st 2022

Abstract

The bilinear-biquadratic spin-1 chain is a striking example of the rich physics encountered in low-dimensional quantum spin systems. The various phases of the model were extensively studied with different analytical and numerical techniques. The interest in spin-1 chains started when Haldane investigated the spin-1 anti-ferromagnetic Heisenberg chain and discovered properties very different from the spin- $\frac{1}{2}$ case[1]. Affleck-Kenedy, Lieb, and Tasaki arrived at a solvable model that includes a bilinear and biquadratic interaction[2][3]. It turned out that both models lie within the same phase, now known as the Haldane phase. The type of order found in the Haldane phase is the first example of symmetry-protected topological order [4]. Most of the early numerical work on this phenomenon was done using exact diagonalization and, more recently, DMRG [5] . Our numerical study of the model relies on Quantum Monte Carlo, more specifically, the worm algorithm in the path Integral representation [6]. The challenge when using Methods is finding a representation free of the negative-sign problem. Only then can an efficient algorithm for calculating physical quantities, like the various order parameters, be found [7]. An appropriate basis transformation can cure the negative-sign-problem. Finding such a transformation often leads to deep physical insight into the nature of the model. In our case, the negative sign fixing transformation is also crucial for understanding symmetry-protected topological order in the Haldane phase [8]. This is undoubtedly the most exciting phenomenon exhibited by the bilinear biquadratic spin-1 model. This thesis is organized as follows: Chapter 1 starts with some basics on Monte Carlo Integration. It ends with an introduction to Quantum Monte Carlo by explaining the worm algorithm. Chapter 2 gives a detailed description of the worm algorithm for the bilinear biquadratic spin-1 model. Chapter 3 is devoted to the AKLT state and the role of entanglement. Finally, in Chapter 4 , we discuss the phase diagram we obtained and compare it with results found by De Chiara et al. [9] using DMRG.

Contents

1	Quantum Monte Carlo	1
1.1	Monte Carlo Integration	2
1.2	Markov Chain Monte Carlo	5
1.3	The Metropolis Algorithm	6
1.4	Monte Carlo Algorithms for the Ising Model	7
	Critical Slowing Down	9
	Worm Algorithm for the 2d Ising Model	9
1.5	From Classical to Quantum Systems	11
1.6	Continous Time Worm Algorithm	14
1.7	Worm Algorithm for the Bose Hubbard Model	15
2	Worm Algorithm for the Bilinear Biquadratic Spin-1 Model	19
2.1	Worm Algorithm for the Heisenberg Model	20
2.2	Monte Carlo Updates for Biquadratic Interactions	21
2.3	Worm Updates	23
	INSERTWORM	24
	MOVEWORM	26
	INSERTKINK/DELETKINK	27
	PASSKINK	28
2.4	The Negative-Sign Problem	28
2.5	Kenedy-Tasaki Transformation and Dimer-R Basis	29
2.6	The 3-Color Bosonic Particle Model	31
3	The AKLT Model and Matrix Product States	35
3.1	Haldane's Conjecture	35
3.2	Entanglement, Area Laws, and Computational Complexity	36
3.3	Matrix Product States	38
3.4	The AKLT Model	39
3.5	Boundary Conditions and Free Edge Spins	42
3.6	Spin-Spin and String Correlation functions	43
4	Phase Diagram	45
4.1	Large-D Phase	46
4.2	Néel Phase	47
4.3	Haldane Phase	48
4.4	Ferromagnetic Phase	49
4.5	The Dimer Phase	51

4.6	Critical Phase	51
5	Conclusion	53
A	Correlation Functions	55

Chapter 1

Quantum Monte Carlo

In this thesis we aim to detect phase transitions in a quantum spin chain, a 1-dimensional system of N interacting quantum spins. Phase transitions occur formally only in the thermodynamic limit: $N \rightarrow \infty$. A phase transition is characterized by an Order Parameter O , which is zero in the disordered phase and non-zero in the ordered phase.

$$\langle O \rangle = \frac{\text{Tr } O e^{-\beta H}}{\text{Tr } e^{-\beta H}} \quad (1.1)$$

We need to find an efficient numerical method to estimate the quantity $\langle O \rangle$ with a given error bound ϵ for large System sizes. We then can infer something about physics in the thermodynamic limit. This task can be formulated rigorously, known as finite-size scaling. But when can we say that we can solve this problem efficiently? This is a question about computational complexity. Following the definition by [10]: *A numerical scheme is said to have a computational complexity Problem (CPP) if the computational time t required to obtain Q with an error ϵ diverges faster than any polynomial function of $\epsilon^{-1} \rightarrow \infty$. The CPP is considered to be solved if $t(\epsilon) = O(\epsilon^{-\alpha})$.* The computational complexity problem occurs in statistical physics because of the scaling of the configuration spaces with the size of the system. The phase space for the classical N -body problem is already $6N$ dimensional. The state-space of a quantum mechanical system grows exponentially in system size. This thesis explores the physics of a 1-dimensional quantum spin chain. The (pure) state of a single spin-1 is described by a state vector in $|\sigma\rangle \in \mathcal{H}$ where the Hilbert space $\mathcal{H} = \mathbb{C}^3$ has dimension 3. If one now takes N such Spins, the Hilbert space for the full system is given by the n -fold tensor product of \mathcal{H} with itself:

$$\mathcal{H}^{\otimes N} \equiv \bigotimes_{i=1}^N \mathcal{H} \quad (1.2)$$

The state-space of the quantum spin-1 chain has therefore $\dim((\mathbb{C}^3)^{\otimes N}) = 3^N$. Just storing the coefficients for a state vector with $N = 25$ requires more than 1 TB of Memory. There are several somewhat different approaches to treat quantum spin chains numerically. Even though it is limited to small System sizes, the method of solving the problem exactly by diagonalizing the full Hamiltonian is still important in the field. In our work, we use this method as a first check

for the Monte Carlo results on small system sizes. We use the Lanczos Algorithm, an efficient algorithm for the diagonalization of sparse Hermitian Matrices. Another group of methods developed in the 1990s and early 2000s relies on the description of quantum spin systems in terms of Matrix-Product-States (MPS). A variety of Algorithms can be formulated in the language of MPS, like the Density-Matrix Renormalization Group (DMRG) for ground-state search and the time-dependent density-matrix renormalization group (tDMRG) for finite temperature physics[11]. DMRG shares some similarities with the exact diagonalization method, as it relies on an iterative procedure for finding the ground state of the quantum spin chain. However, instead of storing the full state, the state is approximated by an MPS. In some unique cases, the ground state is exactly described by a non-trivial MPS. The most famous example is the Affleck-Kennedy-Lieb-Tasaki state, the bilinear-biquadratic spin-1 model for theta = arctan(1/3). Therefore, the Affleck-Kennedy-Lieb-Tasaki model can be used as another benchmark for our Monte Carlo codes. We will describe the AKLT model and the construction of its MPS ground state in some detail in chapter 3. Our numerical studies of the bilinear-biquadratic spin-1 model are based on Quantum Monte Carlo. Quantum Monte Carlo is used for different techniques like Variational Monte Carlo, Diffusion Monte Carlo, or path integral Monte Carlo [12]. We employ the path integral Monte Carlo Method (PIMC), which allows us to estimate finite Temperature correlation Functions for System sizes of $N > 100$, which is far beyond what is possible with exact diagonalization. As the name suggests, PIMC is based on Feynman's path integral formulation of quantum mechanics. This chapter reviews some basic concepts of Monte Carlo Integration and applies these to the classical 2d Ising Model. We then introduce PIMC in the form of the worm algorithm [6].

1.1 Monte Carlo Integration

The Monte Carlo Method is a statistical technique used to evaluate high dimensional integrals or large sums which appear throughout physics and many other disciplines. The method relies on a source of random numbers, or in practice, more commonly on pseudo-random numbers. The first use in physics dates back to the 1940s when the first electronic computers were available at Los Alamos Laboratory [13] [14]. Even though Monte Carlo Methods were first used in high energy physics, they turned out to be very useful for studying low-energy physics as well. The well-known deterministic algorithms for the evaluation of integrals suffer from the so-called curse of dimensionality, which makes them only useful for low dimensional integrals. For high-dimensional integrals, the go-to method is Monte Carlo Integration. In statistical physics, the Quantities of interest often come as integrals over phase space, which is a high-dimensional space. The course of dimensionality can be seen by looking at a simple example, namely an integral of a function f over a hypercube of dimension d:

$$I = \int_{[0,1]^d} f(\vec{x}) d^d x = \int_0^1 \cdots \int_0^1 f(x_1, \dots, x_d) dx_1 \dots dx_d \quad (1.3)$$

Deterministic integration schemes in one dimension rely on quadrature formulas where the function is evaluated on a fixed number of grid points: $n + 1$. The

distance between two neighbouring points is $\Delta \propto n^{-1}$. This discretization introduces a numerical error $\epsilon \propto \Delta^{-1}$. When we generalize the scheme to d dimensions, we need to increase the number of points. For a fixed distance of two neighbouring points, we need to increase the grid points to $(n + 1)^d$. For a fixed error bound, the number of function evaluations grows exponentially. The computational time increases exponentially in the dimension d . The Monte Carlo Method solves this problem by using randomly selected points instead of a fixed mesh. Assume an Integral of the form:

$$I = \langle a \rangle = \int_{\mathbb{R}^d} a(\vec{x}) p(\vec{x}) d^d x \quad (1.4)$$

with $\langle a \rangle < \infty$ and $p(\vec{x})$ a probability density. In order to bring (1.3) into this form we can set $p(\vec{x}) = \mathbb{1}_{[0,1]^d}$ and $a(\vec{x}) = f(\vec{x})$. We now draw N random vectors $\vec{x}^{(1)} \dots \vec{x}^{(N)}$ independent and identically distributed (i.i.d.) from a distribution with probability density $p(\vec{x})$. Then the sample mean gives us an estimate of the integral:

$$\hat{a}_N = \frac{1}{N} \sum_{i=1}^N a(x^{(i)}) \quad (1.5)$$

The weak law of large numbers ensures that for $N \rightarrow \infty$:

$$\hat{a}_N = \frac{1}{N} \sum_{i=1}^N a(x^{(i)}) \xrightarrow{\text{almost surely}} \langle a \rangle \quad (1.6)$$

Given the finite variance of a the central limit theorem states that the distribution of \hat{I}_N converges to normal distribution.

$$\hat{a}_{N \rightarrow \infty} \sim \mathcal{N}(I, \epsilon^2). \quad (1.7)$$

with ϵ^2 , the mean squared error of the estimator \hat{a}_N :

$$\begin{aligned} \epsilon^2 &= \langle [\hat{a}_N - \langle a \rangle]^2 \rangle = \\ &= \left\langle \frac{1}{N^2} \left[\sum_i a(\vec{x}^{(i)}) \right]^2 - \frac{2}{N} \sum_i a(\vec{x}^{(i)}) \langle a \rangle + \langle a \rangle^2 \right\rangle = \\ &= \left\langle \frac{1}{N^2} \sum_i \sum_j a(\vec{x}^{(i)}) a(\vec{x}^{(j)}) \right\rangle^2 - 2 \left\langle \frac{1}{N} \sum_i a(\vec{x}^{(i)}) \right\rangle \langle a \rangle + \langle a \rangle^2 = \\ &= \left\langle \frac{1}{N^2} \sum_i \sum_j [a(\vec{x}^{(i)}) a(\vec{x}^{(j)})]^2 - \langle a \rangle^2 \right\rangle = \\ &= \left\langle \frac{1}{N^2} \sum_i [a(\vec{x}^{(i)})]^2 - \langle a \rangle^2 \right\rangle = \\ &= \frac{1}{N} [\langle a^2 \rangle - \langle a \rangle^2] = \\ &= \frac{1}{N} \text{Var}(a) \end{aligned} \quad (1.8)$$

Now we have the important result that ϵ scales as $N^{-\frac{1}{2}}$ independent of dimension d . We note that the convergence is quite slow, so we need to be very efficient at

generating random numbers. From the principles of quantum mechanics, we know that nature provides us with a way to generate random numbers. Still, physical devices for random number generations have many shortcomings. In practice, we rely on pseudo-random number generators. A pseudo-random number generator is initialized with a number, the so-called seed. Given the seed the algorithm generates a deterministic sequence of numbers $x^{(1)} \dots x^{(N)}$ with $x^{(i)} \in [0, 1]$. There are potential pitfalls when using a pseudo-random number generator regarding their statistical properties, see [15] for more details. Besides their efficiency, there is also another practical advantage. The result of a Monte Carlo simulation becomes reproducible, which makes debugging programs much easier. Coming back to our Integral (1.4) we can now set up a simple algorithm to estimate our Integral. We can generate a random vector in the d-dimensional hypercube using the pseudo-random number generator. The computational cost of generating random vectors scales linearly with dimension. In general, we want to sample according to a probability distribution that is not uniform. For example, we have seen in Equation 1.6 that the mean squared error is proportional to $\text{Var}(a)$. We also note that there is freedom in choosing what $a(x)$ and $p(x)$. In particular, given an integral of the form (1.4), we can choose a suitable $g(x)$ and transform the Integrand:

$$I = \int_{\mathbb{R}^d} d^d x a(\vec{x}) p(\vec{x}) = \int_{\mathbb{R}^d} d^d x \frac{a(\vec{x})}{q(\vec{x})} p(\vec{x}) q(\vec{x}) = \int_{\mathbb{R}^d} d^d x \tilde{a}(\vec{x}) \tilde{p}(\vec{x}) \quad (1.9)$$

we now sample according to the probability distribution with probability density \tilde{p} . we can reduce the mean squared error according to 1.6 by a factor of $\frac{\text{Var}(\tilde{f})}{\text{Var}(f)}$. This assumes that we know that $a(\vec{x})$ is peaked in certain regions, with a suitable $q(\vec{x})$ we can reduce the variance. We next want to consider a case where we integrate over a bounded domain Ω . For simplicity let us assume that $\Omega \subseteq [0, 1]^d$. It might be difficult to directly generate uniformly distributed samples over the domain Ω . We can circumvent this problem by uniformly generating samples according to the uniform distribution over the hypercube and only accepting samples that lie within the domain Ω . This rejection method was already used in the early days of Monte Carlo.[14] One must be aware that rejection sampling can be inefficient for high dimensional integrals. The acceptance probability is given by $q = \frac{\text{Vol}(\Omega)}{\text{Vol}([0, 1]^d)}$. Assume that we want to integrate over the hypersphere $\Omega = S^d$. Then the acceptance probability $q = \frac{4}{3}\pi 2^{-d} \rightarrow 0$ for $d \rightarrow \infty$. This exponential decrease in the acceptance probability leads to an exponential increase in computational time. At this point, it seems as we have just shifted the computational complexity problem to the sample generation. A similar problem also occurs in statistical physics, where uniform sample generation is very inefficient. In principle, one could generate samples uniformly over the phase space and then weigh the configuration by the Boltzmann factor. In the next section, we will see how Markov chains can solve this problem in most cases.

1.2 Markov Chain Monte Carlo

In the previous section, we had the requirement that the random samples be independent and identically distributed (i.i.d.) to use the law of large numbers. However, a Markov chain generates a random sequence where subsequent samples are not independent but correlated. Therefore, we will discuss the conditions under which a Markov chain can be used to construct an unbiased estimator of an integral or a sum. We can motivate Markov chains most easily from a statistical physics point of view. Let us assume we have a classical system with a finite number of Microstates. The states are labeled by $i \in \{0, \dots, m\}$ and have a corresponding Energy E_i . We prepare the system in a random state i_0 and couple it to a heat bath with inverse temperature β . After a sufficiently long time, the system will be in thermal equilibrium with the heat bath. We will measure a state k with probability $\mu_k = \frac{1}{Z} e^{-\beta E_k}$ where $Z = \sum_{i=1}^m E_i$ is the partition function. If we repeat this Experiment N times, we get a sequence of N (i.i.d) random states according to the Boltzmann distribution μ . The thermalization of a physical system is a stochastic process which takes the initial state to the final through a number of intermediate states: $i_0 \rightarrow \dots \rightarrow i_n \rightarrow i_{n+1} \rightarrow \dots \rightarrow k$. Once thermal equilibrium is reached, the system will remain in thermal equilibrium. The idea of Markov chain Monte Carlo (MCMC) is to simulate this process on a computer. It is not important to model the actual physical process as long as it has the desired equilibrium distribution μ . A Markov chain is a very general stochastic process, as it only has one restriction:

$$P[x^{(n+1)} = i_{n+1} | x^{(n)} = i_n, \dots, x^{(0)} = i_0] = P[x^{(n+1)} = j | x^{(n)} = i] \quad (1.10)$$

This is the so-called Markov property. The probability of transitioning from a state i to a state j only depends on the current state i and not on the previous states directly. This property ensures that we decorrelate from the initial state over time. Usually one represents a Markov chain with a graph or with a transition matrix: $P_{ij} = P[x^{(n+1)} = j | x^{(n)} = i]$. The matrix elements are non-negative and specify the Markov chain uniquely. Conservation of probability implies $\sum_j P_{ij} = 1$. The equilibrium distribution is special as it is left invariant by the Markov process. Therefore it is often called stationary or invariant distribution. The stationary distribution is a left eigenvector of the transition matrix with eigenvalue 1:

$$\mu_j = \sum_i \mu_i P_{ij} \quad (1.11)$$

We can find the probability to transition from state i to state j via $(n - 1)$ intermediate states by taking the n th power of the transition matrix: $(P^n)_{ij} = P[x^{(k+n)} = j | x^{(k)} = i]$. An important difference to the direct sampling approach is

that the mean squared error has an additional contribution:

$$\begin{aligned}
& \frac{1}{N^2} \sum_{j \neq i}^N \langle a_i a_j \rangle - \langle a_i \rangle \langle a_j \rangle \\
&= \frac{2}{N^2} \sum_{i < j}^N \langle a_i a_j \rangle - \langle a_i \rangle \langle a_j \rangle \\
&= \frac{2}{N^2} \sum_{i=1}^N \sum_{t=1}^{N-i} (\langle a_i a_{i+t} \rangle - \langle a_i \rangle^2) \\
&= \frac{2}{N^2} \sum_{i=1}^N \sum_{t=1}^{\infty} (\langle a_i a_{i+t} \rangle - \langle a_i \rangle^2) \\
&= \frac{2}{N} \sum_{t=1}^{\infty} (\langle a_i a_{i+t} \rangle - \langle a_i \rangle^2) \\
&= \frac{2}{N} \text{Var}(a) \tau_{int} \quad \text{with } \tau_{int} = \frac{\sum_{t=1}^{\infty} (\langle a_i a_{i+t} \rangle - \langle a_i \rangle^2)}{\text{Var}(a)}
\end{aligned} \tag{1.12}$$

Where τ_{int} is called the integrated autocorrelation time. Adding this contribution to the mean squared error in (1.8), we get the total mean squared error:

$$\epsilon^2 = \frac{1}{N} \text{Var}(a)[1 + 2\tau_{int}] \tag{1.13}$$

1.3 The Metropolis Algorithm

The critical question we still left unanswered is how to find a P which has a given μ as its stationary distribution. Explicit construction of the entire transition matrix is only possible for small state spaces. Furthermore, the equilibrium distribution is often only known up to a normalization factor, which is the partition function in the case of the Boltzmann distribution. The Metropolis Algorithm is the most popular method to construct a Markov chain in such a setting. It is used in almost every modern Monte Carlo Algorithm, even though it has been around for nearly 70 years. The Metropolis Algorithm belongs to a class of Markov Chains that fulfil detailed balance:

$$\mu_j P_{ji} = \mu_i P_{ij} \tag{1.14}$$

This local condition ensures that the global condition (1.11) is satisfied. This can easily be checked:

$$\begin{aligned}
& \mu_j P_{ji} = \mu_i P_{ij} \\
& \Rightarrow \sum_i \mu_j P_{ji} = \sum_i \mu_i P_{ij} \\
& \Leftrightarrow \mu_j \sum_i P_{ji} = \sum_i \mu_i P_{ij} \\
& \Rightarrow \mu_j = \sum_i \mu_i P_{ij}
\end{aligned} \tag{1.15}$$

The main insight of Metropolis et al. [16] was that the transition matrix could be constructed in two steps. We first design a simple probabilistic process, which proposes a transition from state i to state j with probability T_{ij} . In a second step, we accept the proposal with a certain probability p_{ij}^{accept} . If rejected, we remain in state i . The transition matrix is then given by $P_{ij} = T_{ij}p_{ij}^{accept}$. The following choice for p_{ij}^{accept} fulfills detailed balance:

$$p_{ij}^{accept} = \min \left[1, \frac{\mu_j T_{ji}}{\mu_i T_{ij}} \right] \quad (1.16)$$

Metropolis et al. used a symmetric proposal function $T_{ij} = T_{ji}$. The generalization to $T_{ij} \neq T_{ji}$ was introduced by Hastings [17] and went under the name of Metropolis-Hastings.

1.4 Monte Carlo Algorithms for the Ising Model

The 2d classical Ising Model is the prototypical example of a statistical model with a phase transition.

$$H = -J \sum_{i=1}^N \sigma_{i,j} \sigma_{i+1,j} - K \sum_{j=1}^M \sigma_{i,j} \sigma_{i,j+1} \quad (1.17)$$

The state of a classical spin is a binary variable $\sigma = \pm 1$. In our case the spins are placed on a square lattice with $N \times M$ sites and periodic boundary conditions in both dimensions, i.e. $\sigma_{N+1,j} = \sigma_{1,j}$ and $\sigma_{i,M+1} = \sigma_{i,1}$. We will label the spin configurations by a matrix Λ with matrix elements $[\Lambda]_{ij} = \sigma_{i,j}$. We note that the Hamiltonian is invariant under the transformation $\Lambda \rightarrow -\Lambda$. Formally this is known as the discrete \mathbb{Z}_2 symmetry. For positive coupling constants, $J_1 > 0$ and $J_2 > 0$, the system undergoes a phase transition. It is in a disordered phase at high temperature and in an ordered phase below a critical temperature T_c . Onsager [18] was the first to solve the problem. He found an analytical solution for the critical temperature T_c :

$$\sinh\left(\frac{2J}{kT_c}\right) \sinh\left(\frac{2K}{kT_c}\right) = 1 \quad (1.18)$$

The phase transition is a result of symmetry breaking. For example, in the case of the 2d Ising model, the \mathbb{Z}_2 is broken below T_c . Landau was the first to introduce a rigorous theoretical framework for studying classical phase transitions. The breaking of the symmetry happens only in the infinite size System. One can add an external field term $H_b = b \sum_{i=1}^N \sum_{j=1}^M \sigma_{i,j}$ which explicitly breaks the \mathbb{Z}_2 symmetry. By first taking the thermodynamic limit and then taking the limit $b \rightarrow 0$, one can see that the symmetry is broken below T_c even when the external field is absent. Landau [19] famously introduced the concept of an order parameter, a physical quantity by which one can detect the phase transition. The order parameter can either change discontinuously (first-order) or continuously (second-order) as one varies the temperature. The phase transition in the Ising model is of second order. These phase transitions have a diverging correlation length at T_c . One of the reasons why

the Ising model is interesting is that it can be solved analytically. It is, therefore, an ideal testbed for MCMC. We can design an Algorithm and compare the results against the analytical solutions. Of course, the quantity we would like to estimate is the order parameter. In the case of the 2d Ising model, this is the mean squared magnetization. For a configuration Λ this is given by:

$$M^2(\Lambda) = \left[\frac{1}{NM} \sum_{i=1}^N \sum_{j=1}^M \sigma_{i,j} \right]^2 \quad (1.19)$$

The ground states of the system $[\Lambda]_{ij} = +1$ and $[\Lambda]_{ij} = -1 \forall i, j$ break the \mathbb{Z}_2 system. At high temperatures, the system is disordered, and the \mathbb{Z}_2 symmetry is not broken. The system has a second-order phase transition from a ferromagnetic to a paramagnetic phase. The quantity (1.19) can be used as an order parameter to detect the transition from the ferromagnetic to the paramagnetic phase. At an inverse temperature β , the mean squared magnetization is given by:

$$\langle M^2 \rangle = \frac{1}{Z} \sum_{\sigma} M^2(\sigma) e^{-\beta E_{\sigma}} \quad (1.20)$$

We can now use the Metropolis Algorithm to estimate the quantity $\langle M^2 \rangle$. We start with a arbitrary Spin configuration σ^0 . We then randomly choose a site i where we propose a spin flip: $\sigma^0 = (\sigma_1, \dots, \sigma_i, \dots, \sigma_N) \rightarrow \sigma^1 = (\sigma_1, \dots, -\sigma_i, \dots, \sigma_N)$. This proposal function is symmetric so the acceptance probability just contains the Boltzmann weights of the two configurations:

$$p^{accept} = \min \left[1, \frac{e^{-\beta E_{\sigma^1}}}{e^{-\beta E_{\sigma^0}}} \right] = \min \left[1, e^{-\beta \Delta E} \right] \quad (1.21)$$

The algorithm is ergodic as any configuration can be reached by a finite number of

+ + + - + + - + + -	+ + + - + + - + + -
- - + - + + + + + +	- - + - + + + + + +
+ + + + + + + + + -	+ + + + + + + + + -
+ + - - - - - + + +	+ + - - + - - + + +
- + - + - - + + + -	- + - + - - + + + -
+ + + + - + + - + +	+ + + + - + + - + +
+ + - + - - - + - -	+ + - + - - - + - -
+ - - + + - - + - +	+ - - + + - - + - +
+ + + + - + + - + -	+ + + + - + + - + -
+ - + - + - + + - +	+ - + - + - + + - +

→

Figure 1.1. The energy difference ΔE only depends on the four bonds where the spin is flipped. For this configuration the energy is raised for three bonds while it is lowered for one: $\Delta E = 3\beta - 1\beta = 2\beta$. We therefore only accept the move with probability $e^{-2\beta}$

spin flips, and the weight of all configurations is non-vanishing for $\beta < \infty$. Therefore, we can be sure that the state will be decorrelated from the starting configuration after some time.

Critical Slowing Down

If we look at a typical spin configuration near the critical point, we see the formation of domains in which spins are aligned. In the spin-flip algorithm we choose randomly which spin to flip. Most likely, the spin will have all its neighbours aligned, which means that the acceptance ratio will be small. Even if the flip is accepted, when spin is chosen the next time, it will be flipped back again. Only when a spin at a domain wall is chosen do we have a high acceptance ratio. It, therefore, takes a long time to flip a cluster of spins. This phenomenon is known as critical slowing down. It is a problem that typically occurs when we use local updates at second-order phase transitions. For the Ising model, the critical slowing down can be avoided by using the famous Wolff Algorithm. In this algorithm, larger groups of spins can be flipped simultaneously. We will, although, follow a different route and discuss the worm algorithm, which is similarly successful at sampling near the second-order phase transitions.

Worm Algorithm for the 2d Ising Model

It was believed for a long time that local Metropolis Algorithms for the classical Ising model are plagued by critical slowing down. In the 1990s, the worm algorithm, first used for quantum Models, proved this belief wrong. Apart from using local Metropolis updates, it is very different from the spin-flip algorithm discussed before. The spin-flip algorithm was inspired by the physical process, where thermal fluctuations cause random spin flips which drive the system to thermal equilibrium. The real power of MCMC lies in the fact that we can use it quite generally to sample large sums or integrals. One can combine MCMC with any technique where large Sums or high dimensional integrals appear. For the 2d classical Ising model, we can combine MCMC with the high-temperature Series expansion. Later we will use MCMC to sample path integrals for 1d quantum spin chains. Even though the systems and the techniques are different, we can use a very similar algorithm. In both cases, the partition function can be expressed as a sum of closed path configurations. These closed path configurations are sampled efficiently by the worm algorithm. The worm algorithm was invented by Prokofiev and Svistunov for quantum Systems [6] and later extended for classical systems [20]. Among them was also the 2d classical Ising model. We now consider the isotropic case of (1.17), i.e. $J = K$. For the isotropic it is most convenient to use a sum over bonds $b = \langle i, j \rangle$. The partition function factorizes as a product over bonds:

$$Z = \sum_{\Lambda} e^{-\beta H} = \sum_{\Lambda} e^{\beta \sum_{\langle i,j \rangle} J \sigma_i \sigma_j} = \sum_{\Lambda} \left(\prod_{b=\langle i,j \rangle} e^{\beta J \sigma_i \sigma_j} \right) \quad (1.22)$$

In the next step, we expand in powers of βJ . Again, the Ising model is special as only zeroth and first-order survive:

$$\begin{aligned} e^{\beta J \sigma_i \sigma_j} &= \sum_{k=0}^{\infty} \frac{(\beta J)^k}{k!} (\sigma_i \sigma_j)^k = \sum_{k=0}^{\infty} \frac{(\beta J)^{2k}}{2k!} \underbrace{(\sigma_i \sigma_j)^{2k}}_{=1} + \sum_{k=0}^{\infty} \frac{(\beta J)^{2k+1}}{2k+1!} \underbrace{(\sigma_i \sigma_j)^{2k+1}}_{=\sigma_i \sigma_j} = \\ &= \cosh(\beta J) + \sinh(\beta J) \sigma_i \sigma_j = \cosh(\beta J) [1 + \tanh(\beta J) \sigma_i \sigma_j] \end{aligned}$$

$$Z = 2^{NM} \cosh^{2NM}(K) \sum_{\Lambda} \left(\prod_{\langle i,j \rangle} [1 + \tanh(\beta J) \sigma_i \sigma_j] \right) \quad (1.23)$$

We now introduce a new binary variable called the bond occupation number $N_b \in \{0, 1\}$.

$$Z = 2^{NM} \cosh^{2NM}(K) \sum_{\Lambda} \left(\prod_{\langle i,j \rangle} \sum_{N_{i,j} \in \{0,1\}} [\tanh(\beta J) \sigma_i \sigma_j]^{N_{i,j}} \right) \quad (1.24)$$

Similar to the summation over Spin configurations in the previous section, we can now rewrite it as a sum over bond configurations, with the difference that most bond configurations have zero weight. This can be seen by picking a specific site k . We define n_k as the sum of occupied bonds incident on-site k : $n_k = \sum_l N_{l,k}$. The partition function contains a sum over all possible values of σ_k :

$$Z \sim \sum_{\sigma_k \in \{-1, +1\}} (\sigma_k)^{n_k} \quad (1.25)$$

For an odd value of n_k we get two terms which exactly cancel out. Only bond configurations with an even number of bonds incident on each site have non-zero weight. Bond configuration satisfying this condition from closed paths. From a Monte Carlo perspective, arises an interesting question: can we find a Markov chain that samples from the space of closed path configurations according to the partition function. One could approach this task similar to the sampling of spin configurations in the previous section. We start with a certain loop configuration and locally deform it. Then we use the Metropolis Algorithm to accept or reject the proposed deformation. One of the conditions we have to satisfy is ergodicity. We are actually sampling loop configurations on a torus, not on a plane, when using periodic boundary conditions. If we start with a loop configuration that winds around the torus, we can not locally deform it to a configuration that does not wind around the torus. This is an ergodicity problem. Prokofiev et al. solved this by introducing configurations with two open ends. This can be achieved by "deleting" an occupied bond or occupying a previously empty bond. The two open ends are called the worm head and tail. We visually represent the site where the head and tail reside with a square and a dot, respectively. One chooses randomly which open end is the head and which is the tail. The worm algorithm performs local Metropolis updates on the worm head. The worm head can move to one of the four neighbouring sites. A move always has a non-zero acceptance probability. The new configuration has two open ends again unless we propose moving to the site where the worm tail resides. In that case, we get a new closed path configuration, which contributes to the partition function. This local update scheme allows us to solve the ergodicity problem described previously. We can reach any closed path configuration independent of our starting configuration. The only price we have to pay is that the open path configurations do not contribute to the partition function. At first sight, this seems to be a significant drawback of the worm algorithm. It turns out that the configurations with two open ends also sample a physical quantity, namely the spin-spin correlation function. A histogram of the



Figure 1.2. The worm algorithm allows open-loop (a) configurations to overcome the ergodicity problem. Configuration (b) contributes to the partition function.

worm head and tail distance is an estimator for the spin-spin correlation function. A diverging correlation length characterizes a second-order phase transition. Instead of estimating the mean squared magnetization, we can use the spin-spin correlation function to detect the phase transition in the Ising model. The fact that the worm algorithm directly samples the diverging correlation function at the phase transition is what makes it so efficient.

1.5 From Classical to Quantum Systems

It was not obvious that Monte Carlo Methods could be applied to quantum systems. As a matter of fact, Metropolis et al. assumed classical Statistics in their 1953 paper. Coincidentally, the same year, Richard Feynman introduced the path integral formulation of quantum mechanics [21]. In the following decades, Feynman's formulation became very useful for the numerical study of strongly correlated quantum systems. Again we use the Monte Carlo Method to sample finite temperature expectation values. Even though we now want to detect quantum phase transitions that occur at zero temperature, i.e., in the limit $\beta \rightarrow \infty$. In the same way, as we used finite-size scaling to study the limit $N \rightarrow \infty$, we can also use scaling arguments for this limit. The first PIMC Algorithm used a discrete path integral representation of the partition function. The trace of the density matrix gives the quantum mechanical partition function:

$$Z = \text{Tr}\{e^{-\beta H}\} = \text{Tr}\{\rho\} \quad (1.26)$$

Finite temperature expectation values of on operator \hat{O} is given by:

$$\langle \hat{O} \rangle = \frac{1}{Z} \text{Tr}[\hat{O}\hat{\rho}] \quad (1.27)$$

We will use the canonical basis set $\{|\boldsymbol{\sigma}\rangle\}$ which is a short hand notation for the tensor product of the local S^z basis $\{|\sigma\rangle\}$:

$$|\boldsymbol{\sigma}\rangle := |\sigma_1\rangle \otimes \dots \otimes |\sigma_N\rangle \quad (1.28)$$

In the field of quantum Monte Carlo, this is often called the computational basis. Quantum Monte Carlo can be used for quantum spin models as well as fermionic and bosonic models on a lattice. A simple quantum spin model is the transverse field Ising Model:

$$H = -J \sum_i \sigma_i^z \sigma_{i+1}^z - \sum_i \Gamma \sigma_i^x \quad (1.29)$$

It can be seen as a quantum version of the classical Ising model with an additional transverse field term. The first part of the Hamiltonian $H_0 = -J \sum_i \sigma_i^z \sigma_{i+1}^z$ is diagonal in the computational basis. For $\Gamma = 0$, the problem is equivalent to the classical Ising model in one dimension. We could straightforwardly apply the Monte Carlo methods discussed so far. Only when the off-diagonal part $H_I = -\Gamma \sum_i \sigma_i^x$ is present we have a true quantum problem. In PIMC, we make use of the fact that the Hamiltonian can always be split in the off-diagonal H_I and diagonal part H_0 . There are different implementations of PIMC. We will first discuss the discrete version and then move one to the more modern continuous worm algorithm. In the former, one starts a rewriting of the density matrix at inverse temperature β as a product of density matrices at inverse temperature $\epsilon_\tau = \frac{\beta}{M}$:

$$Z = \text{Tr}\{e^{-\beta H}\} = \text{Tr}\left\{\prod_{m=1}^M e^{-\epsilon_\tau H}\right\} \quad (1.30)$$

The next one inserts a sum over the full basis set between the operators.

$$Z = \sum_{\boldsymbol{\sigma}^1, \dots, \boldsymbol{\sigma}^M} \langle \boldsymbol{\sigma}^0 | e^{-\epsilon_\tau H} | \boldsymbol{\sigma}^M \rangle \dots \langle \boldsymbol{\sigma}^1 | e^{-\epsilon_\tau H} | \boldsymbol{\sigma}^0 \rangle \quad (1.31)$$

At this point there are different possibilities how to proceed. In PIMC we treat the diagonal part exactly and make an expansion in the off-diagonal terms. We here use the Suzuki-Trotter decomposition [22] and a linear expansion in H_I . When $H_I = \sum_{i=1}^N h_i$ is a sum of local operators we use the following decomposition:

$$e^{-\epsilon_\tau H} = e^{-\frac{\epsilon_\tau H_0}{2}} e^{-\epsilon_\tau H_I} e^{-\frac{\epsilon_\tau H_0}{2}} = \sum_{i=1}^N e^{-\frac{\epsilon_\tau H_0}{2}} (1 - \epsilon_\tau h_i) e^{-\frac{\epsilon_\tau H_0}{2}} \quad (1.32)$$

In the limit $M \rightarrow \infty$, we get an exact rewriting of the partition function.

$$Z = \lim_{M \rightarrow \infty} \left(\sum_{\boldsymbol{\sigma}^1, \dots, \boldsymbol{\sigma}^M} \prod_{m=0}^{M-1} e^{-\frac{\epsilon_\tau}{2} [E_{diag}(\boldsymbol{\sigma}^{m+1}) + E_{diag}(\boldsymbol{\sigma}^m)]} \langle \boldsymbol{\sigma}^{m+1} | (1 - \epsilon_\tau H_I) | \boldsymbol{\sigma}^m \rangle \right) \quad (1.33)$$

With $E_{diag}(\boldsymbol{\sigma}) = \langle \boldsymbol{\sigma} | H_0 | \boldsymbol{\sigma} \rangle$ and $|\boldsymbol{\sigma}^{M+1}\rangle = |\boldsymbol{\sigma}^1\rangle$. Compared to the classical partition function we have an additional index m . This can be seen as an additional dimension.

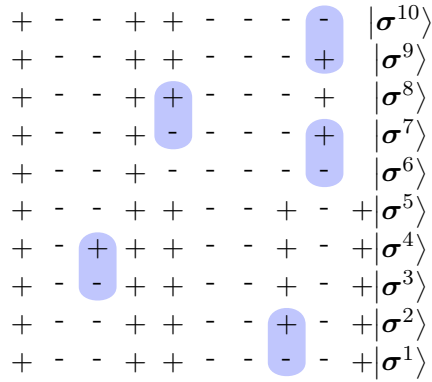


Figure 1.3. The 1D transverse field Ising model is equivalent to the 2d classical Ising Model. At the coloured bonds, there is a spin-flip, which means that the contribution to the partition function is $\epsilon_\tau \Gamma$.

The density operator $\rho = e^{-\beta H}$ is formally equivalent to the time evolution operator $U(0, t) = e^{-itH}$ with $t = i\tau$. We therefore call this additional dimension the imaginary time. We can use the same numerical Methods for time evolution and finite temperature physics. The important difference is that there are periodic boundary conditions in the imaginary time direction due to the trace in (1.30). Suzuki was the first to show that a d dimensional quantum system can mapped onto a d+1 dimensional classical system. We will now look in more detail at the 1d transverse field Ising model:

Here the off-diagonal part of the Hamiltonian is a sum of local operators: $H_I = \sum_{i=1}^N h_i$.

$$H_I = \sum_{i=1}^N H_i. \text{ with } [H_i, H_j] = 0 \text{ for } i \neq j \quad (1.34)$$

We can approximate the partition function Z by a discretized partition function Z_M , with $Z = \lim_{M \rightarrow \infty} Z_M$. For the transverse field Ising model, the discretized partition function is given by:

$$Z_M = \sum_{\sigma^1, \dots, \sigma^M} \prod_{m=1}^M e^{-\frac{\epsilon_\tau}{2} [E_{diag}(\sigma^{m+1}) + E_{diag}(\sigma^m)]} \prod_{n=1}^N \langle \sigma_n^{m+1} | (1 + \epsilon_\tau \Gamma S^x) | \sigma_n^m \rangle \quad (1.35)$$

Simillarly to the spin-flip Algorithm we can sample 2d spin configurations Section 1.5. We can define the discretized path integral also for other quantum spin systems like the XXZ model:

$$H = -J \sum_i [S_j^x S_{j+1}^x + S_j^y S_{j+1}^y] - J_z \sum_i S_j^z S_{j+1}^z \quad (1.36)$$

This leads to path configuration similar to the one we found when discussing the worm algorithm, see Section 1.5. Historically the discretization of the path integral was the first implementation of Quantum Monte Carlo. Nowadays, continuous-time path integrals are more widely used. We will therefore not discuss this in more detail for the discrete case.

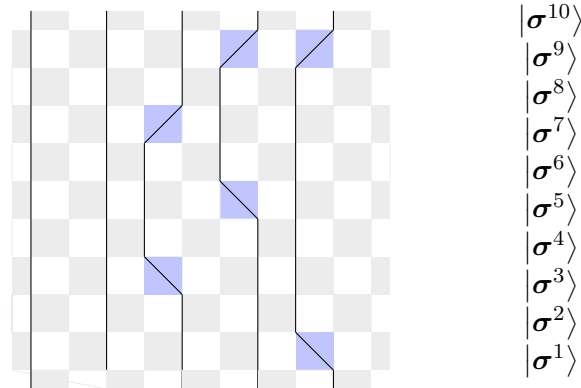


Figure 1.4. Path integral in discrete time for the XXZ model

1.6 Continous Time Worm Algorithm

Path integral Monte Carlo can be derived directly in continuous time, avoiding the discretization error. In fact, the continuous-time formulation is numerically exact [23], which allows us to construct unbiased estimators for the partition function and different observables. We already mentioned how time evolution and finite temperature are related. Therefore, it is no surprise that we can use the techniques for finding solutions for the time-dependent schrödinger equation in the current setting. Whenever we can split the Hamiltonian into a part \mathcal{H}_0 for which we know the eigenstates and a more difficult part \mathcal{H}_1 , it is convenient to use the interaction representation. This representation is commonly used in quantum field theory, and it is usually the starting point for time-dependent perturbation theory. The formalism can be found in many standard textbooks we follow [24] and define the interaction picture states and operators as:

$$\text{States: } |\hat{\psi}(t)\rangle \equiv e^{i\mathcal{H}_0 t}|\psi(t)\rangle$$

$$\text{Operators: } \hat{O}(t) \equiv e^{i\mathcal{H}_0 t} O e^{-i\mathcal{H}_0 t}$$

Operators and states without the hat are the states and operators in the Schrödinger picture where only the states evolve in time. The Schrödinger equation in the interaction picture is given by

$$\partial_t |\hat{\psi}(t)\rangle = \hat{\mathcal{H}}_1(t) |\hat{\psi}(t)\rangle \quad (1.37)$$

with $\hat{\mathcal{H}}_1(t) = e^{i\mathcal{H}_0 t} \mathcal{H}_1 e^{-i\mathcal{H}_0 t}$. One then introduces a time evolution operator $U(t, t_0)$ which describes the evolution of $|\hat{\psi}(t)\rangle$ from a initial time t_0 through $|\hat{\psi}(t)\rangle = \hat{U}(t, t_0) |\hat{\psi}(t_0)\rangle$. Inserting $|\hat{\psi}(t)\rangle = e^{i\mathcal{H}_0 t} e^{-iHt} |\psi_0\rangle$ and equivalently for $|\hat{\psi}(t_0)\rangle$ we find:

$$\hat{U}(t, t_0) = e^{i\mathcal{H}_0 t} e^{-iH(t-t_0)} e^{-i\mathcal{H}_0 t_0} \quad (1.38)$$

The Schrödinger equation can now be expressed in terms of $\hat{U}(t, t_0)$:

$$i\partial_t \hat{U}(t, t_0) = \hat{\mathcal{H}}_1 \hat{U}(t, t_0) \quad (1.39)$$

Or equivalently via the Integral equation:

$$\hat{U}(t, t_0) = 1 - i \int_{t_0}^t dt_1 \hat{\mathcal{H}}_1(t_1) \hat{U}(t_1, t_0) \quad (1.40)$$

The reason to formulate time evolution via the Integral equation is that we can find the solution for $\hat{U}(t_1, t_0)$ iteratively:

$$\begin{aligned} \hat{U}(t_1, t_0) &= 1 - i \int_{t_0}^t dt_1 \hat{\mathcal{H}}_1(t_1) + (-i)^2 \int_{t_0}^t dt_1 \hat{\mathcal{H}}_1(t_1) \int_{t_0}^{t_1} dt_2 \hat{\mathcal{H}}_1(t_2) + \dots \\ &= 1 + \sum_{n=1}^{\infty} (-i)^n \int_{t_0}^t dt_1 \int_{t_0}^{t_1} dt_2 \dots \int_{t_0}^{t_{n-1}} dt_n \hat{\mathcal{H}}_1(t_1) \hat{\mathcal{H}}_1(t_2) \dots \hat{\mathcal{H}}_1(t_n) \end{aligned} \quad (1.41)$$

The operators in the second line are time ordered. We now turn our attention back to the density operator. The time evolution operator \hat{U} can be related to the imaginary time evolution operator $\hat{\sigma}$ by a Wick rotation: $it \rightarrow \tau$. This operator is often referred to as the Matsubara evolution operator. We now follow the original formulation of the worm algorithm by Prokofiev et al.[6]. Using (1.38) we can write the density operator as $e^{-\beta H} = e^{-\beta \mathcal{H}_0} \hat{\sigma}(0, \beta)$, and find a solution for $\hat{\sigma}(0, \beta)$ iteratively just as in (1.41):

$$\begin{aligned} \hat{\sigma}(0, \beta) &= 1 - \int_0^\beta d\tau_1 \hat{\mathcal{H}}_1(\tau_1) + \int_0^\beta d\tau_1 \hat{\mathcal{H}}_1(\tau_1) \int_0^{\tau_1} d\tau_2 \hat{\mathcal{H}}_1(\tau_2) + \dots \\ &= 1 + \sum_{n=1}^{\infty} (-1)^n \int_0^\beta d\tau_1 \int_0^{\tau_1} d\tau_2 \dots \int_0^{\tau_{n-1}} d\tau_n \hat{\mathcal{H}}_1(\tau_1) \hat{\mathcal{H}}_1(\tau_2) \dots \hat{\mathcal{H}}_1(\tau_n) \end{aligned} \quad (1.42)$$

The expansion of the partition function is hence given by:

$$Z = \text{Tr } e^{-\beta \mathcal{H}_0} \sum_{n=0}^{\infty} \int_0^\beta d\tau_1 \int_0^{\tau_1} d\tau_2 \dots \int_0^{\tau_{n-1}} d\tau_n \hat{\mathcal{H}}_1(\tau_1) \dots \hat{\mathcal{H}}_1(\tau_n) \quad (1.43)$$

We have now arrived at an expression that can be sampled using a Markov chain. Here we both have a sum and high-dimensional integral. Similar to the discrete case, we insert a complete basis set between the interaction picture operators. Again each configuration can be represented graphically. For this, we consider a concrete example, namely the Bose-Hubbard model.

1.7 Worm Algorithm for the Bose Hubbard Model

The Bose-Hubbard model is one of the prime examples which shows the power of path integral Monte Carlo. The worm algorithm is the most efficient method for estimating finite temperature expectation values. Critical slowing down near the Mott insulator to superfluid transition is almost absent. The interest in the Bose-Hubbard model is largely driven by the developments in cold atom experiments over the last decades. The Bose-Hubbard model was experimentally realized in optical lattices [25]. At the same time, the system sizes realized in experiments are accessible to the worm algorithm numerically. The Bose Hubbard Hamiltonian reads:

$$H = \sum_{i=1}^N \mathcal{H}_{i,i+1} + \sum_{i=1}^N h_i = - \sum_i^N t [b_i^\dagger b_{i+1} + b_{i+1}^\dagger b_i] + \sum_i^N \frac{U}{2} n_i(n_i - 1) - \sum_i^N \mu_i n_i \quad (1.44)$$

For the Bose-Hubbard model, one typically chooses the local occupation number basis $\{|n_1\rangle_1 \otimes |n_2\rangle_2 \otimes |n_3\rangle_3 \otimes \cdots \otimes |n_N\rangle_N\}$ as the computational basis. We will use the short hand notation $\{|n_1, n_2, \dots, n_N\rangle\}$. The kinetic part $\mathcal{H}_1 = t[b_i^\dagger b_j + b_j^\dagger b_i]$ of the Hamiltonian (1.44) is then off-diagonal, and the rest of the Hamiltonian is diagonal. The kinetic part with the coupling constant t causes transitions between states in the computational basis. The transitions can be interpreted as hopping events of particles. The expansion order n in eq. 1.63 are the number of hopping events present in a worldline configuration.

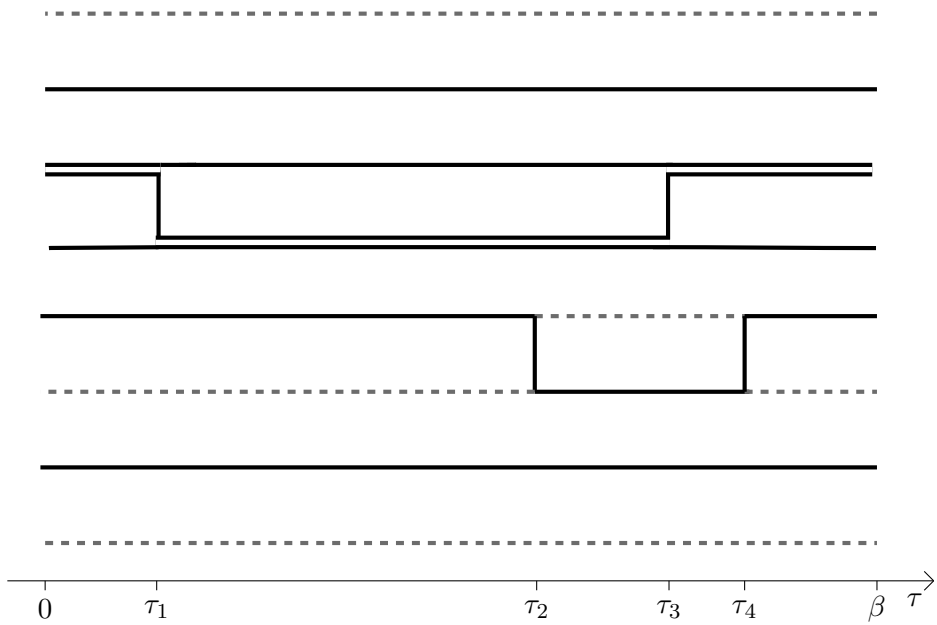


Figure 1.5. Closed path configuration with four hopping events, we will also refer to these events as kinks.

The weight of such a world line configuration can be determined by inserting a full basis set between each $\hat{\mathcal{H}}_1$ in (1.44). We denote the diagonal part of the Energy as $E_{i_k} = \mathcal{H}_0|i_k\rangle$. The weight W_n of a configuration is given by [26] :

$$W_n = \langle i_1 | \mathcal{H}_1 | i_2 \rangle e^{-(\tau_2 - \tau_1)E_{i_2}} \langle i_2 | \mathcal{H}_1 | i_3 \rangle e^{-(\tau_3 - \tau_2)E_{i_3}} \dots e^{-(\tau_n - \tau_{n-1})E_{i_n}} \langle i_n | \mathcal{H}_1 | i_1 \rangle e^{-(\beta + \tau_1 - \tau_n)E_{i_1}} \quad (1.45)$$

Similarly to the worm algorithm for the Ising model, the algorithm samples in an extended space with open worldline configurations. The space of open worldline configurations is called the Greens function sector. In this sector, we sample the finite-temperature, single-particle greens function[26] :

$$G_{ij}(\tau) = Z^{-1} \text{Tr} \left[\mathcal{T} \left((b_i(t_0)b_j^\dagger(\tau) + \text{h.c.}) \exp(-\beta H) \right) \right] \quad (1.46)$$

The weight W_n^G of a configuration in the Greens function sector is given by:

$$\begin{aligned} W_n^G = & \langle i_1 | \mathcal{H}_1 | i_2 \rangle e^{-(\tau_2 - \tau_1)E_{i_2}} \langle i_2 | \mathcal{H}_1 | i_3 \rangle e^{-(\tau_3 - \tau_2)E_{i_3}} \dots \\ & \dots e^{-(\tau_k - \tau_{k-1})E_{i_k}} \langle i_k | b_i^\dagger | i_{k+1} \rangle \dots \\ & \dots e^{-(\tau_l - \tau_{l-1})E_{i_k}} \langle i_l | b_j | i_{l+1} \rangle \dots \\ & e^{-(\tau_n - \tau_{n-1})E_{i_n}} \langle i_n | \mathcal{H}_1 | i_1 \rangle e^{-(\beta + \tau_1 - \tau_n)E_{i_1}} \end{aligned} \quad (1.47)$$

We are mainly interested in the equal time Greens function $G_{ij}(0)$. The remaining task is to determine the Monte Carlo updates to generate all possible configurations. This is again done by local Metropolis updates on the worm head. Conceptually, this is very similar to the worm algorithm for the two-dimensional Ising model. The important difference is that we have a continuous dimension in the current

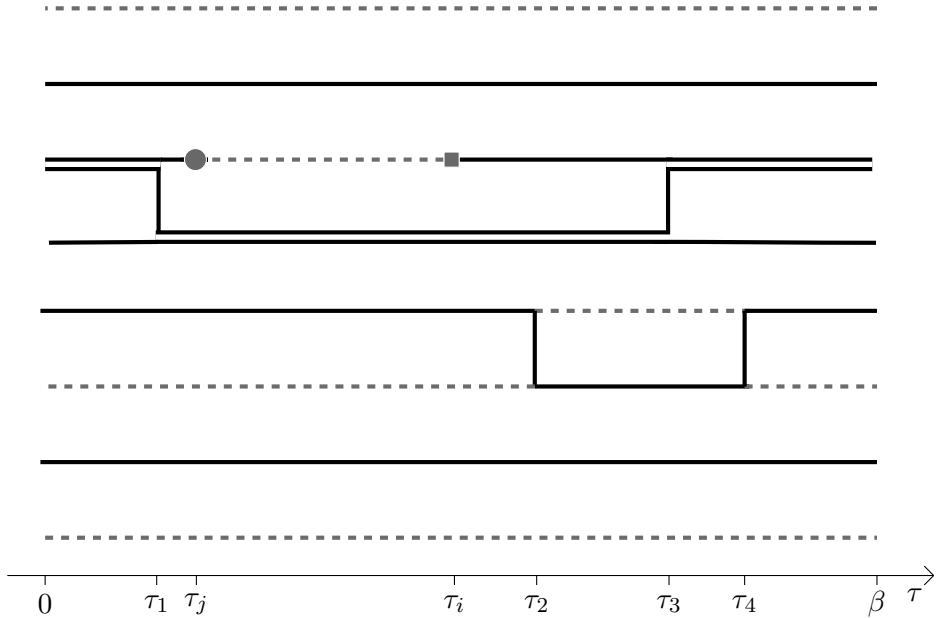


Figure 1.6. Open path configuration, containing a so-called worm. The worm head and tail are again labelled using a square and a dot.

setting. The difficulty lies in generating closed path configurations and moves when the time dimension is continuous. This is technically much more difficult than in the discrete case. Furthermore, one has some freedom in designing the algorithm. The algorithm we employ is in some details different from the original algorithm described by Prokovief et al. [6]. The next chapter will give a detailed description of the worm algorithm for the bilinear biquadratic spin-1 model. We will see how the one-dimensional Bose-Hubbard model is related to quantum spin chains.

Chapter 2

Worm Algorithm for the Bilinear Biquadratic Spin-1 Model

We will now apply the worm algorithm to the bilinear biquadratic spin-1 chain with an uniaxial anisotropy:

$$H = \sum_{i=1}^{N-1} \mathcal{H}_{i,i+1} + \sum_{i=1}^N h_i = \sum_{i=1}^{N-1} \gamma \vec{S}_i \otimes \vec{S}_{i+1} + \alpha (\vec{S}_i \otimes \vec{S}_{i+1})^2 + \sum_{i=1}^N D(S_i^z)^2 \quad (2.1)$$

There are three free parameters: the bilinear coupling constant γ , the biquadratic coupling constant α and the on-site anisotropy parameter D . This system is entirely different from the Bose Hubbard model. Still, there is an almost one-to-one correspondence between the Bose Hubbard model and the antiferromagnetic Heisenberg model from an algorithmic perspective. The antiferromagnetic Heisenberg model is the case $\alpha = 0$ and $\gamma < 0$ in (2.1). The vital difference is that the local Hilbert space has a finite dimension in the case of spin models $\dim(H) = 2S + 1$ and is infinite in the case of the Bose Hubbard model. This property can be readily implemented in the worm algorithm for the Bose Hubbard model by constraining the local occupation number. Only when the biquadratic term is present ($\alpha \neq 0$), the algorithm needs to be modified significantly. There are two challenges when designing an algorithm for the bilinear-biquadratic spin-1 chain:

1. The presence of both a bilinear and biquadratic interaction increases the complexity of the worm updates.
2. The negative-sign problem arises for certain choices of γ and α

For a part of the parameter region, the negative sign problem can be cured by a transformation reminiscent of the non-local Jordan Wigner transformation. This leads to a new model with different worm updates, which is in some ways different from the algorithm for the Bose-Hubbard model. For other choices of γ and α , one can use local transformations to arrive at a negative-sign free model. The transformations lead to different models with various types of interactions, making the present chapter rather technical. We first describe the worm algorithm for the

original bilinear-biquadratic spin-1 model and then discuss the algorithm for the transformed Hamiltonian, which is just an extension of the worm algorithm for the Bose-Hubbard model.

2.1 Worm Algorithm for the Heisenberg Model

We recall the Hamiltonian of the Bose-Hubbard Model:

$$H = \sum_{i=1}^N \mathcal{H}_{i,i+1} + \sum_{i=1}^N h_i = - \sum_i^N t[b_i^\dagger b_{i+1} + b_1^\dagger b_i] + \sum_i^N \frac{U}{2} n_i(n_i - 1) - \sum_i^N \mu_i n_i \quad (2.2)$$

The limit $U \rightarrow \infty$ (hard-core boson limit) leads to a model which can be associated with the Spin- $\frac{1}{2}$ Heisenberg model. The occupation number is either 0 or 1, which can be associated with spin up or down. When not within this limit, the occupation number is unbounded. The implementation of the worm algorithm still has a cut-off boson occupation number n_{max} . This cut-off has purely technical reasons. With $n_{max} = 2$, the Bose Hubbard model has a local Hilbert space of dimension 3, like a spin-1 model. Different from the spin- $\frac{1}{2}$ case, we can not directly associate the bilinear coupling constant γ in (2.1) with the hopping amplitude t in (2.2), this is due to different commutation relations of boson and spin operators. Still, the Hamiltonians have the same non-vanishing off-diagonal matrix elements if we restrict ourselves to the case $\alpha = 0$ and $\gamma < 0$, i.e. the antiferromagnetic Heisenberg model. Let us explicitly compare the off-diagonal matrix elements of (2.1) and (2.2) for the case $\alpha = 0$. We use the local occupation number as our computational basis for the Bose Hubbard model. For convenience we define $\mathcal{H}_{\text{off}} = \mathcal{H}_{i,i+1} - \text{diag}(\mathcal{H}_{i,i+1})$ = for both (2.1) and (2.2). For the Bose Hubbard model with $n_{max} = 2$ we get:

$$\mathcal{H}_{\text{off}} = \begin{pmatrix} \langle 00| & \langle 01| & \langle 02| & \langle 10| & \langle 11| & \langle 12| & \langle 20| & \langle 21| & \langle 22| \\ |00\rangle & \left(\begin{array}{ccccccccc} 0 & 0 & 0 & 0 & 0 & 0 & 0 & 0 & 0 \\ 0 & 0 & 0 & -\frac{1}{2}t & 0 & 0 & 0 & 0 & 0 \\ 0 & 0 & 0 & 0 & -\frac{1}{\sqrt{2}}t & 0 & 0 & 0 & 0 \\ 0 & -\frac{1}{2}t & 0 & 0 & 0 & 0 & 0 & 0 & 0 \\ 0 & 0 & -\frac{1}{\sqrt{2}}t & 0 & 0 & 0 & -\frac{1}{\sqrt{2}}t & 0 & 0 \\ 0 & 0 & 0 & 0 & 0 & 0 & 0 & -t & 0 \\ 0 & 0 & 0 & 0 & -\frac{1}{\sqrt{2}}t & 0 & 0 & 0 & 0 \\ 0 & 0 & 0 & 0 & 0 & -t & 0 & 0 & 0 \\ 0 & 0 & 0 & 0 & 0 & 0 & 0 & 0 & 0 \end{array} \right) & (2.3) \end{pmatrix}$$

For the antiferromagnetic Heisenberg model, we use the local S^z basis as the compu-

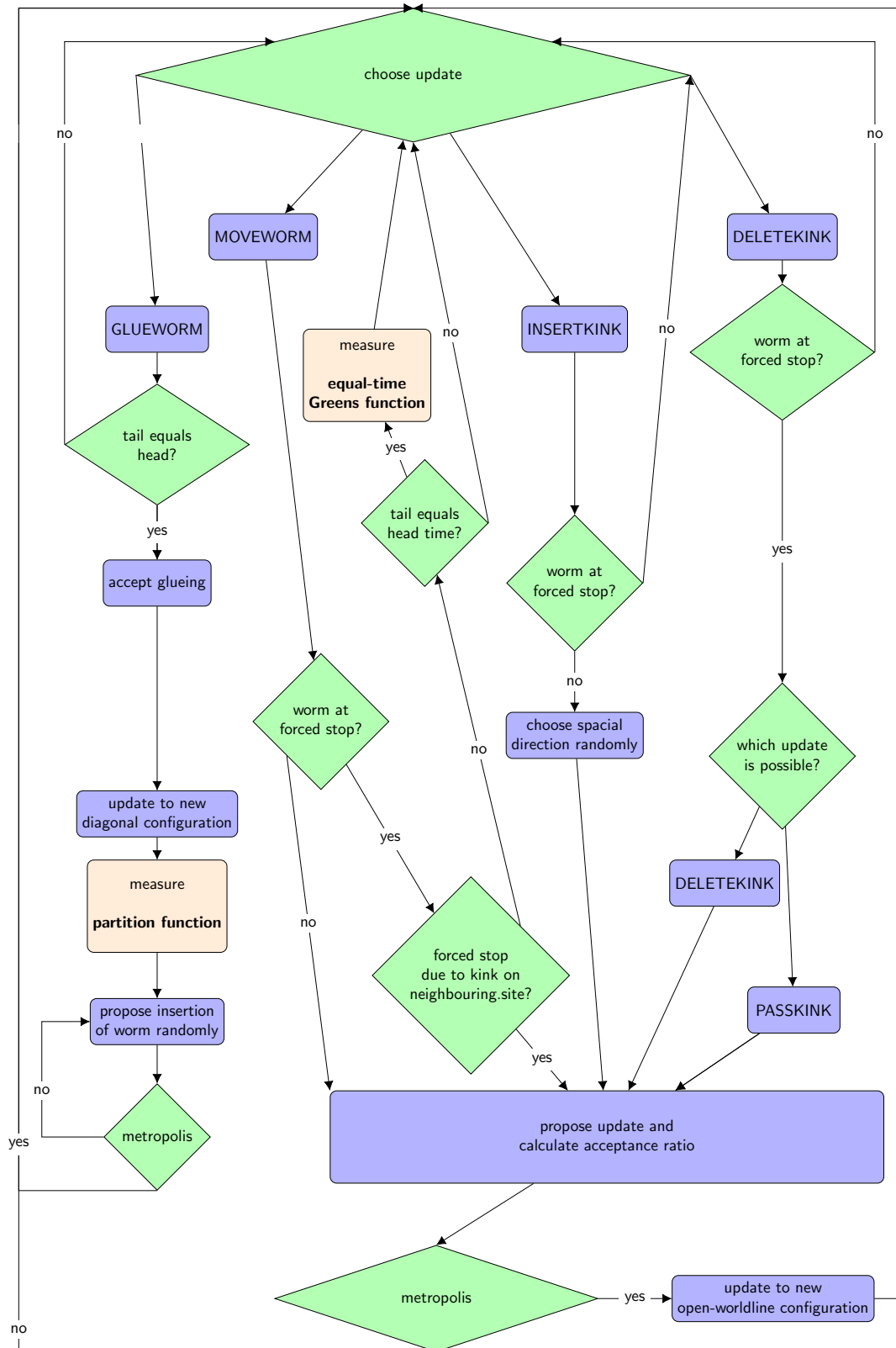
tational basis:

$$\mathcal{H}_{\text{off}} = \begin{pmatrix} \langle--| & \langle-0| & \langle-+| & \langle0-| & \langle00| & \langle0+| & \langle+-| & \langle+0| & \langle++| \\ |--\rangle & 0 & 0 & 0 & 0 & 0 & 0 & 0 & 0 \\ |-0\rangle & 0 & 0 & 0 & \gamma & 0 & 0 & 0 & 0 \\ |-+\rangle & 0 & 0 & 0 & 0 & \gamma & 0 & 0 & 0 \\ |0-\rangle & 0 & \gamma & 0 & 0 & 0 & 0 & 0 & 0 \\ |00\rangle & 0 & 0 & \gamma & 0 & 0 & 0 & \gamma & 0 \\ |0+\rangle & 0 & 0 & 0 & 0 & 0 & 0 & 0 & \gamma \\ |+-\rangle & 0 & 0 & 0 & 0 & \gamma & 0 & 0 & 0 \\ |+0\rangle & 0 & 0 & 0 & 0 & 0 & \gamma & 0 & 0 \\ |++\rangle & 0 & 0 & 0 & 0 & 0 & 0 & 0 & 0 \end{pmatrix} \quad (2.4)$$

The similar form of (2.1) and (2.2) lead to an almost one-to-one correspondence between the Bose-Hubbard model and antiferromagnetic Heisenberg model. From now on, we will use occupation numbers to describe the worm algorithm for the Heisenberg model even though we do not use the occupation number basis but the S^z basis. It is easier to think in terms of hopping events. We notice that the hopping term in (2.2) and the bilinear interaction in (2.1) both cause transitions from states $|n, m\rangle$ to states $|n \pm 1, m \mp 1\rangle$. Importantly one has additional factors of $\frac{1}{2}$ and $\frac{1}{\sqrt{2}}$ in the case of the Bose Hubbard model. The problem is negative-sign free in the ferromagnetic case $\gamma < 0$. In the antiferromagnetic case $\gamma > 0$, the negative-sign problem can be cured by a local basis change, at least for bipartite lattices[27]. A spin chain with an even number of sites is bipartite. The transformation only acts one every second spin. The possible world line configurations are thus all positive. The worm algorithm for the Bose Hubbard model and various Spin models, which share the same type of updates as the Heisenberg model and the XXZ model. These models are extensively described in the literature [28] [26]. The continuous-time worm algorithm described in Section 1.6 and Section 1.7 can therefore be used with minimal modifications for the antiferromagnetic Heisenberg model. In particular, one can think of occupation numbers and hopping events also for the Heisenberg model and use a graphical representation for the open-worldline and closed world line configurations in Figure 1.6 and Figure 1.5 respectively.

2.2 Monte Carlo Updates for Biquadratic Interactions

The following section will discuss the worm algorithm updates for the spin-1 Heisenberg model with bilinear and biquadratic Interactions. To treat the biquadratic term, we need to extend the algorithm. The model is negative-sign free for $\gamma \leq \alpha \leq 0$. Just as for the case $\alpha = 0$ we restrict the occupation number per site to $n_{\max} = 2$. We discussed the hoping term in the Bose Hubbard model and the bilinear coupling constant in the Heisenberg model, which causes transitions from states $|n\rangle|m\rangle$ to $|n \pm 1\rangle|m \mp 1\rangle$. The constant γ can be associated with the hopping amplitude t in the Bose Hubbard Hamiltonian. When the biquadratic interaction ($\alpha \neq 0$) is present we have additional non-zero off-diagonal matrix elements. Transitions from states $|n\rangle|m\rangle$ to states $|n \pm 2\rangle|m \mp 2\rangle$ are also possible. Even though such interactions are usually not considered in bosonic particle models, we will still use the particle



language to describe the algorithm for the bilinear-biquadratic spin-1 model. The matrix elements of the two-body Hamiltonian in (2.1) are given by:

$$\mathcal{H}_{i,i+1} = \begin{pmatrix} \langle 00| & \langle 01| & \langle 02| & \langle 10| & \langle 11| & \langle 12| & \langle 20| & \langle 21| & \langle 22| \\ |00\rangle & \gamma & 0 & 0 & 0 & 0 & 0 & 0 & 0 \\ |01\rangle & 0 & 0 & 0 & \gamma & 0 & 0 & 0 & 0 \\ |02\rangle & 0 & 0 & \alpha - \gamma & 0 & \gamma - \alpha & 0 & \alpha & 0 \\ |10\rangle & 0 & \gamma & 0 & 0 & 0 & 0 & 0 & 0 \\ |11\rangle & 0 & 0 & \gamma - \alpha & 0 & \alpha & 0 & \gamma - \alpha & 0 \\ |12\rangle & 0 & 0 & 0 & 0 & 0 & 0 & 0 & \gamma \\ |20\rangle & 0 & 0 & \alpha & 0 & \gamma - \alpha & 0 & \alpha - \gamma & 0 \\ |21\rangle & 0 & 0 & 0 & 0 & 0 & \gamma & 0 & 0 \\ |22\rangle & 0 & 0 & 0 & 0 & 0 & 0 & 0 & \gamma \end{pmatrix} \quad (2.5)$$

The basic structure of the worm algorithm is unchanged. It is, although technically, more difficult to implement the algorithm. In the following section, we will describe the updates in more detail, with a focus on how one can generate all possible worldline configurations with both types of interactions. In Figure 2.1 we can see a possible closed-worldline configuration.

2.3 Worm Updates

Let us assume we have a valid open-world line configuration as in Figure 1.6. We then perform updates on the worm head, i.e. it performs a random walk through spacetime. During this random walk, we have different possibilities to update a configuration. We can move in time (MOVEWORM), jump to a neighbouring site, and create a new kink (INSERTKINK). When the head encounters a kink, there are several options (DELETEKINK) or a change in the type of kink. When the worm head meets the worm tail, the world line is "glued together" (GLUEWORM), and we get a closed worldline configuration as in Figure 1.5. Then we insert a new worm (INSERTWORM) and again perform a random walk. Before delving into the details of the different updates, it is crucial to emphasize the fact that the worm algorithm is a local algorithm. If we propose an update from a state A to a state B , we use the Metropolis-Hastings Algorithm to accept/reject the update. The quantity that goes into the acceptance probability is the relative weight of the two configurations, i.e. the ratio $W(A)/W(B)$. The two configurations only differ by a local worm move. In a single update, the worm moves at most to the neighbouring site or stays on-site and moves in imaginary time. The Hamiltonian is restricted to nearest neighbour and on-site interactions. We only need to consider occupations and kinks at the site of the worm head and the two neighbouring sites. In implementing the worm algorithm, we use a data structure that allows us to access this local information. There is no general best practice on how to do this. It mainly depends on the programming languages used and the data structures available. Our algorithm is written in $C++$ and uses the standard list provided by $C++$. There is a dedicated list for each lattice site that contains all of the kinks ordered in time. Each list item contains the following information: the occupation before the kink, the occupation after the kink, the type of kink and the site to which it is linked. Additionally, the item contains a reference to the kink on the neighbouring sites, which is just greater in time. In

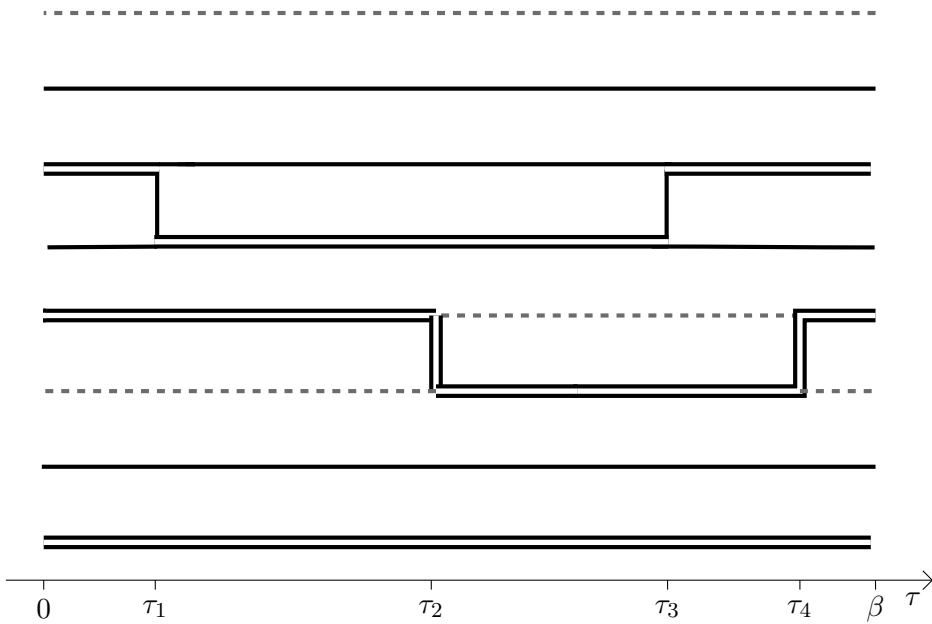


Figure 2.1. A possible closed path configuration for a model with both bilinear and biquadratic interactions.

an update, one needs to read/delete/insert new items at the site of the worm head and the neighbouring site. One needs to iterate through the items in a list to access specific information. The reference to the kinks on the neighbouring sites reduces the number of iterations performed in each update. The code heavily relies on list iterators and pointers to store the reference to the neighbouring kinks. Another peculiarity that needs to be considered when storing a configuration is that the time dimension is continuous. We can only store the time variables with finite-precision on a computer. We use the double format, which can store a floating-point number with approximately 16 significant digits precision. We can therefore only differentiate two times τ_1 and τ_2 if their difference is above a certain threshold, in our case we use $|\tau_1 - \tau_2| > \beta \cdot 10^{-15} = \Delta\tau_{min}$. The discretization error is therefore not completely absent in the worm algorithm. Next, we will describe the updates in more detail. For a complete description of the design of the proposal function and how to satisfy detailed balance, we refer to [26] [6]. We focus more on the differences introduced by the biquadratic coupling. The different types of updates we describe in the rest of the section are chosen with a probability that the user can set. These probabilities are one of the few optimization parameters the user can select.

INSERTWORM

To generate interactions with an occupation number difference of 1 and 2, we will allow two types of worms. The occupation number can change by ± 1 or ± 2 at the worm ends. We will call these worms of charge 1 and 2, respectively, and the corresponding interactions type 1 and 2. Choosing two different types of open-worldlines is not strictly necessary to arrive at an algorithm that ergodically samples the partition function. As noted by Prokoviev and Svistunov, there is some freedom when designing the algorithm[6] :

The worm algorithm idea is to consider an enlarged configuration space that includes structures violating constraints present in the Z-sector of the space. Often, this can be achieved automatically by considering the relevant correlation functions. Greens function and, for paired states, higher-order off-diagonal correlators are the appropriate choice for the path-integral space. However, one should feel free to introduce unphysical configurations which bear no meaning at all and are used solely for employing local updates to produce non-trivial global changes of physical configurations.

In the INSERTWORM update, we randomly select the occupation number between the worm head and tail. Any occupation number $0 \leq n \leq 2$ which differs from the occupation number at the insertion point is allowed. In Figure 2.2 we see the two different possibilities we have when inserting a new worm. It should be noted that

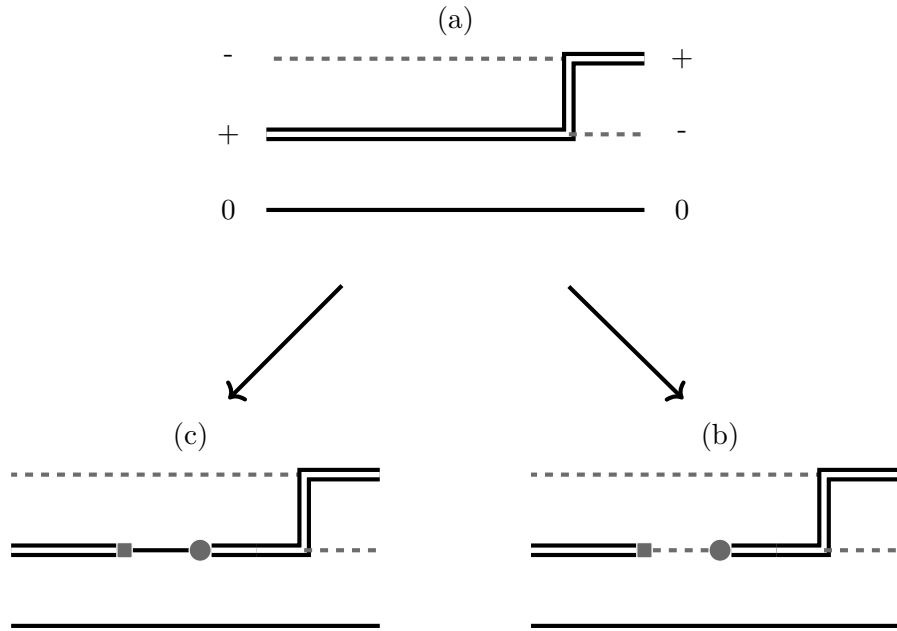


Figure 2.2. When inserting a worm starting from the closed path configuration (a), there are two possible occupation numbers.

we sample different correlation functions in cases (b) and (c). The relative weights of (b) and (c) differ in the number of spin-raising and lowering operators and samples, therefore, different physical quantities:

$$W_b = \langle i_k | S_j^+ | i_{k+1} \rangle \langle i_{k+1} | S_{j+1}^- | i_{k+2} \rangle \quad (2.6)$$

$$W_c = \langle i_k | (S_j^+)^2 | i'_{k+1} \rangle \langle i'_k | (S_{j+1}^-)^2 | i_{k+1} \rangle \quad (2.7)$$

The inverse to the INSERTWORM update is called GLUEWORM. The glueing of the worm head and tail is possible whenever the worm head encounters the tail, i.e. they need to be at the same site and be infinitesimally close. This problem will be discussed in the following subsection.

MOVEWORM

Next, we discuss the possible updates after a worm was inserted. The first type of update we consider is a move in time. Just as with the worm algorithm for the Ising model, we only move the worm head. At the worm's insertion, we randomly choose which end is the head and which is the tail. We then stick to this choice until we arrive at a new close world-line configuration. For now, we assume that the head resides at a site j and time τ_w . The MOVEWORM update consists of the following steps: first, a random direction is chosen with equal probability. We assume for now that the positive time direction was chosen. We note that the system is invariant under time reversal. Next we check if a move is possible. For example, if the worm head is located at a kink or at the worm tail, we can not just move past it. For now we assume that we move is possible and that the next interaction is at time τ_{int} with time $\tau_i - \tau_w > \Delta\tau_{min}$. In this update, we generate an exponentially distributed number that goes into the proposal function. If the proposed time τ'_w satisfies the condition $\tau'_w - \tau_w < \Delta\tau_{min}$ the move can be accepted. The Metropolis algorithm is used to accept or reject the move. It is important to note that neighbouring kinks also affect the relative weight of the new configuration. This is only the case when the Hamiltonian contains a diagonal nearest neighbour interaction. Consider the case where $\tau'_w - \tau_w > \Delta\tau_{min}$ in Figure 2.4: the configuration (a) and (c) have the following relative weights:

$$W_a = e^{-\tau_w E_{i_k}} \langle i_k | S_j^+ | i_{k+1} \rangle e^{(\tau_w - \tau_0) E_{i_{k+1}}} \langle i_{k+1} | (S_{j+1}^-)^2 (S_{j+2}^+)^2 | i_{k+2} \rangle e^{\tau_0 E_{i_{k+2}}} \quad (2.8)$$

$$W_c = e^{-\tau_0 E_{i_k}} \langle i_k | (S_{j+1}^-)^2 (S_{j+2}^+)^2 | i'_{k+1} \rangle e^{(\tau_0 - \tau'_w) E_{i'_{k+1}}} \langle i'_k | S_j^+ | i_{k+1} \rangle e^{\tau'_w E_{i_{k+2}}} \quad (2.9)$$

We notice that the diagonal Energy changes when we move past τ_i . In our implementation, we force the worm to stop. We can only move past τ_i in a subsequent update when a move in the same time direction is proposed. This peculiarity in the design of the worm algorithm and how to satisfy detailed balance is described in detail in [26]. A so-called forced stop is not only required in the instance we have just mentioned but also when:

1. A kink at the site of the worm is encountered

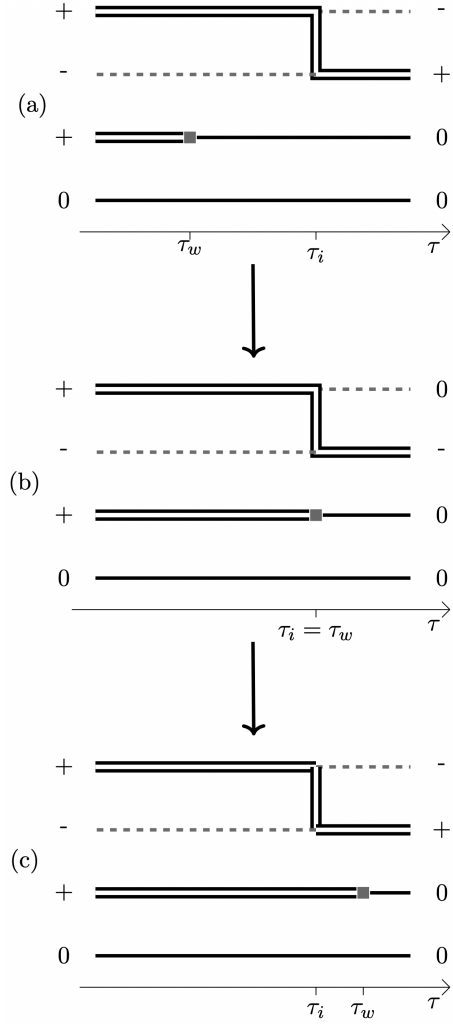


Figure 2.3. Head moves past kink

2. The worm head moves past the worm tail in time.

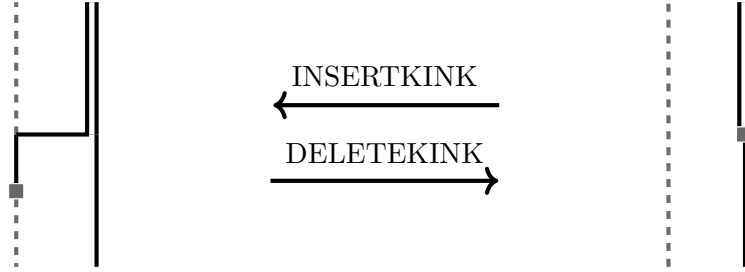


Figure 2.4. The insertion of a kink and its reverse is the kink's deletion.

While (1) is required to satisfy detailed balance, instance (2) might be less obvious. Indeed (2) is necessary for measuring a physical quantity, namely the equal time Greens function [26]. In our case, we sample the following off-diagonal correlation function:

$$C_{ij} = \langle S_i^+ S_j^- + S_i^- S_j^+ \rangle \quad (2.10)$$

INSERTKINK/DELETKINK

A crucial set of updates are the ones that change the number of changes in a world line configuration. We first discuss the INSERTKINK update, which increases the number of kinks by one. The update is possible whenever we have an open worldline configuration where the worm head is not at a forced stop. The worm head can then jump to one of the two neighbouring sites, chosen with equal probability. The insertion of the kink will always be rejected if it would result in a negative occupation number or if it would be larger than n_{max} . The INSERTKINK update, also has

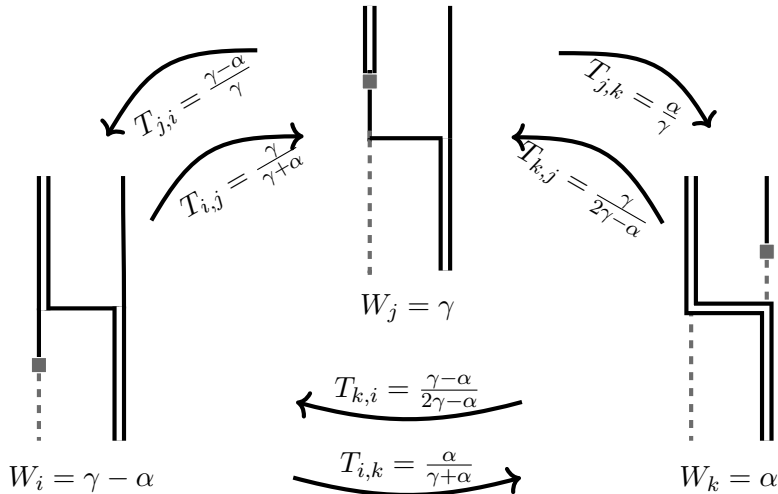


Figure 2.5. The relative weights and transition probabilities for the process where the kink can be passed or modified.

an inverse process: DELETKINK. This update is possible when the worm halts at

an interaction that can be deleted. In some instances, deletion of the kink is not possible. Then the worm head can bounce back or pass the kink. In the presence of both bilinear and biquadratic interactions, there are even more possibilities.

PASSKINK

The main difference in the Algorithms for the model with or without biquadratic interactions are in the updates where the worm encounters an interaction. For the bilinear biquadratic spin-1 Hamiltonian, there are additional off-diagonal Elements and, therefore, additional cases one must consider. One needs to draw all possible kinks and all possible worms and check which moves are allowed. Most of these cases are very similar to the ones in the Bose-Hubbard model, especially the ones where the worm has charge 2. A few cases are very different, and one has to think about how to reach all states without violating overall balance. These 6 cases are depicted in [Figure 2.5](#) and [Figure 2.7](#). The processes split into two groups of 3. We explicitly give the relative weights and the transition probability we have chosen. In principle, one could use the Metropolis Algorithm to fulfil detailed balance. It is although easy to verify that the algorithm is balanced with the transition probabilities we use. A special property of these processes is that the worm head can pass the interaction, i.e. the number of kinks remains unchanged, but the type of kink changes. In this process, the worm can jump to a neighbouring site.

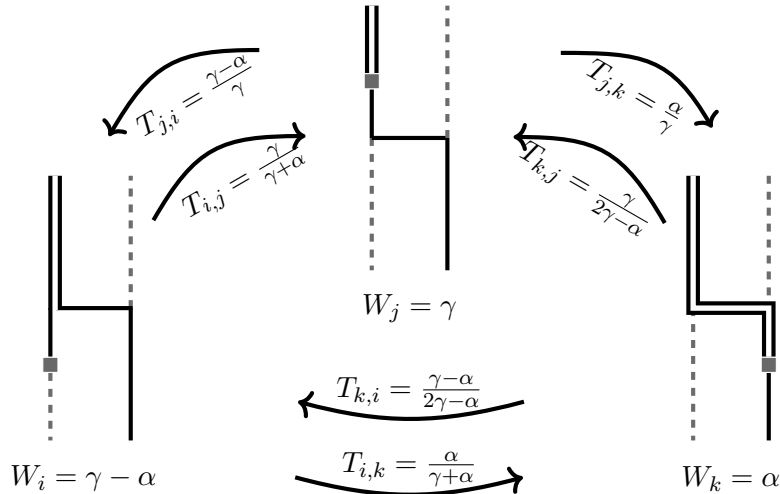


Figure 2.6. The relative weights and transition probabilities for the process where the kink can be passed or modified.

2.4 The Negative-Sign Problem

This section will discuss the negative-sign problem arising in the bilinear biquadratic spin-1 model. The off-diagonal matrix elements of [\(2.5\)](#) are non-positive for $\gamma < \alpha < 0$. If this condition is not met, the negative-sign problem does not allow an efficient sampling of expectation values. In the literature, we find various transformations that cure the negative-sign problem for most parameter choices. [Table 2.1](#) gives

an overview of the known transformations. Still, there remains a case for which no sign-curing transformation was found. We will discuss the transformations (b)

Parameter	negative-sign curing transformation
(a) $\gamma < \alpha < 0$	no negative-sign problem
(b) $\alpha < \gamma < 0$	A local basis transformation can cure the negative sign-problem, see [29]. Bipartiteness and open boundary conditions are not required.
(c) $0 < \gamma$ and $\alpha < \gamma$	Kennedy-Tasaki transformation followed by the R-Dimer basis, see[30] . Bipartiteness is not required.
(d) $0 < \gamma$ and $\alpha = 0$	On bipartite lattices, a rotation on every second site can remove the negative-sign, see [27][31]
(e) $0 < \alpha$ and $\gamma < \alpha$	No transformation known.

Table 2.1. Negative-sign curing transformations for the bilinear biquadratic spin-1 model

and (c) in this thesis. They will both lead to the same bosonic particle model. Transformation (d) is not discussed, as this parameter choice can also be covered by (c).

2.5 Kenedy-Tasaki Transformation and Dimer-R Basis

In the following subsection, we closely follow Okunishi et al.[30]. We will reiterate the key points relevant to our purpose. For the detailed discussion and extension of the Method, we refer to the original work by Okunishi et al. The negative-sign problem is removed in two steps first the Kennedy Tasaki transformation is applied:

$$\mathcal{U} = \prod_{\langle i,j \rangle} U_{i,j} \quad (2.11)$$

with $i < j$:

$$U_{i,j} = e^{i\pi S_i^z S_j^x} \quad (2.12)$$

The unitary $U_{i,j}$ act as a pair disentanglers, i.e. they transform the entangled ground states of the AKLT model in to product states: $|\psi_{AKLT}^{\downarrow\uparrow}\rangle, |\psi_{AKLT}^{\uparrow\downarrow}\rangle, |\psi_{AKLT}^{\uparrow\uparrow}\rangle, |\psi_{AKLT}^{\downarrow\downarrow}\rangle$. These states are described in [Section 3.5](#). The transformed states have the following from and are explicitly given in Okunishi et al.:

$$|\Phi^\nu\rangle = \prod_i |\phi_i^\nu\rangle \quad (2.13)$$

The ground states are again four-fold degenerate:

$$\begin{aligned} |\phi^1\rangle &= \frac{1}{\sqrt{3}}(|1\rangle + |2\rangle + |3\rangle) \\ |\phi^2\rangle &= \frac{1}{\sqrt{3}}(|1\rangle - |2\rangle + |3\rangle) \\ |\phi^3\rangle &= \frac{1}{\sqrt{3}}(|1\rangle + |2\rangle - |3\rangle) \\ |\phi^4\rangle &= \frac{1}{\sqrt{3}}(|1\rangle - |2\rangle - |3\rangle) \end{aligned} \quad (2.14)$$

We note that these states possess ferromagnetic order in contrast to the hidden antiferromagnetic order present before the transformation, see [Section 3.5](#). The Kennedy-Tasaki transformation not only allows us to disentangle the AKLT ground states but also removes the negative sign problem. For this we need to perform an additional local transformation. For this purpose the local dimer-R basis is introduced:

$$V_i = \begin{pmatrix} \frac{1}{\sqrt{2}} & 0 & -\frac{1}{\sqrt{2}} \\ \frac{1}{\sqrt{2}} & 0 & \frac{1}{\sqrt{2}} \\ 0 & 1 & 0 \end{pmatrix} \quad (2.15)$$

The transformation is local because it acts on each site individually. The basis-transformation on the full system is simply given by $\mathcal{V} = \prod_i V_i$. Combining this transformation with the Kennedy Tasaki transformation denoted by \mathcal{U} we recover a negative-sign free Hamiltonian when the condition in (c) of [Table 2.1](#) is satisfied :

$$\tilde{H} = \mathcal{V}\mathcal{U}H\mathcal{U}^\dagger\mathcal{V}^\dagger \quad (2.16)$$

The Kennedy-Tasaki transformation has the special property that it preserves the property of the Hamiltonian that it only includes nearest-neighbour interactions. In general, a non-local transformation on a Hamiltonian with nearest neighbour interactions can lead to long-range interactions. We do not explicitly carry out the calculation of the matrix elements. We refer to the original work by Okunishi et al. The resulting two-body Hamiltonian is given by:

$$\tilde{\mathcal{H}}_{i,i+1} = \begin{pmatrix} \langle 00| & \langle 01| & \langle 02| & \langle 10| & \langle 11| & \langle 12| & \langle 20| & \langle 21| & \langle 22| \\ |00\rangle & \alpha & 0 & 0 & -\gamma + \alpha & 0 & 0 & 0 & -\gamma + \alpha \\ |01\rangle & 0 & 0 & 0 & -\gamma & 0 & 0 & 0 & 0 \\ |02\rangle & 0 & 0 & 0 & 0 & 0 & 0 & -\gamma & 0 \\ |10\rangle & 0 & -\gamma & 0 & 0 & 0 & 0 & 0 & 0 \\ |11\rangle & -\gamma + \alpha & 0 & 0 & 0 & \alpha & 0 & 0 & -\gamma + \alpha \\ |12\rangle & 0 & 0 & 0 & 0 & 0 & 0 & -\gamma & 0 \\ |20\rangle & 0 & 0 & -\gamma & 0 & 0 & 0 & 0 & 0 \\ |21\rangle & 0 & 0 & 0 & 0 & 0 & -\gamma & 0 & 0 \\ |22\rangle & -\gamma + \alpha & 0 & 0 & 0 & -\gamma + \alpha & 0 & 0 & \alpha \end{pmatrix} \quad (2.17)$$

When the parameters satisfy condition (b) of Table 2.1 we can use a different type of local transformation. Kaul et al. [29] introduce the following local transformation:

$$W_i = \begin{pmatrix} -i/\sqrt{2} & 0 & i/\sqrt{2} \\ 1/\sqrt{2} & 0 & 1/\sqrt{2} \\ 0 & i & 0 \end{pmatrix} \quad (2.18)$$

It is discussed by Okunishi et al., although not for the purpose of curing the negative sign problem in parameter region (b). Again we transform the full chain with $\mathcal{W} = \prod_i W_i$. This time we just use \mathcal{W} without any additional non-local transformation:

$$\hat{H} = \mathcal{W} H \mathcal{W}^\dagger \quad (2.19)$$

The transformed Hamiltonian leads to the same effective model as the previous transformation, there is only a different sign for certain off-diagonal elements of the Hamiltonian:

$$\hat{\mathcal{H}}_{i,i+1} = \begin{matrix} & \langle 00 | & \langle 01 | & \langle 02 | & \langle 10 | & \langle 11 | & \langle 12 | & \langle 20 | & \langle 21 | & \langle 22 | \\ \begin{array}{c} |00\rangle \\ |01\rangle \\ |02\rangle \\ |10\rangle \\ |11\rangle \\ |12\rangle \\ |20\rangle \\ |21\rangle \\ |22\rangle \end{array} & \left(\begin{array}{cccccccc} \alpha & 0 & 0 & 0 & -\gamma + \alpha & 0 & 0 & 0 & -\gamma + \alpha \\ 0 & 0 & 0 & \gamma & 0 & 0 & 0 & 0 & 0 \\ 0 & 0 & 0 & 0 & 0 & 0 & \gamma & 0 & 0 \\ 0 & \gamma & 0 & 0 & 0 & 0 & 0 & 0 & 0 \\ -\gamma + \alpha & 0 & 0 & 0 & \alpha & 0 & 0 & 0 & -\gamma + \alpha \\ 0 & 0 & 0 & 0 & 0 & 0 & 0 & \gamma & 0 \\ 0 & 0 & \gamma & 0 & 0 & 0 & 0 & 0 & 0 \\ 0 & 0 & 0 & 0 & 0 & \gamma & 0 & 0 & 0 \\ -\gamma + \alpha & 0 & 0 & 0 & -\gamma + \alpha & 0 & 0 & 0 & \alpha \end{array} \right) \end{matrix} \quad (2.20)$$

We now arrived at a negative-sign free representation via a local as well as a non-local basis transformation. Next, we will discuss these transformed Hamiltonians in more detail.

2.6 The 3-Color Bosonic Particle Model

The Hamiltonian in (2.17), as well as (2.20), lead to a bosonic particle model. The basis states $|0\rangle$, $|1\rangle$ and $|2\rangle$ can be associated with three different colours red, green and blue. The two types off-diagonal elements proportional to $\pm\gamma$ and $\alpha - \gamma$ can be associated with an exchange process and a pair creation and annihilation process.

After transforming to the negative-sign free basis, the string correlation function corresponds to an off-diagonal two-point correlation function. The String correlation function can be estimated by making a histogram of the worm head and tail distance [30] whenever they are at equal times:

$$\left\langle S_i^z e^{i\pi \sum_{i < k < j} S_k^z} S_j^z \right\rangle_{\mathcal{H}} = -\left\langle T_i^z T_j^z \right\rangle_{\tilde{\mathcal{H}}} \quad (2.21)$$



Figure 2.7. There are two types of kinks for the 3-color bosonic particle model, a particle exchange process and a pair creation-annihilation process.

Four, the original Hamiltonian, which includes a magnetic field term in the z-direction, we would also like to measure the Spin-Spin correlation function.

$$\langle S_i^z S_j^z \rangle_{\mathcal{H}} = - \left\langle T_i^z e^{i\pi \sum_{i < k < j} T_k^z} T_j^z \right\rangle_{\tilde{\mathcal{H}}} \quad (2.22)$$

Due to its non-local structure, estimating this correlation function is less straightforward. To see how we can consider the extra phase factors can be seen in the graphical representation. Following the convention of [30] we assign colors to the three different basis states ($|0\rangle$ - red, $|1\rangle$ - green, $|2\rangle$ blue). The operators in Dirac notation are given by $T^z = |01\rangle\langle 10| + |10\rangle\langle 01|$ and $e^{i\pi T^z} = |00\rangle\langle 00| + |11\rangle\langle 11| - |22\rangle\langle 22|$.

Differently from the histogram for the String-correlation function where we just have a counter for each distance which is increased by +1 whenever it occurs, it can now change by a continuous value between +1 and -1 depending on the occupation between head and tail.

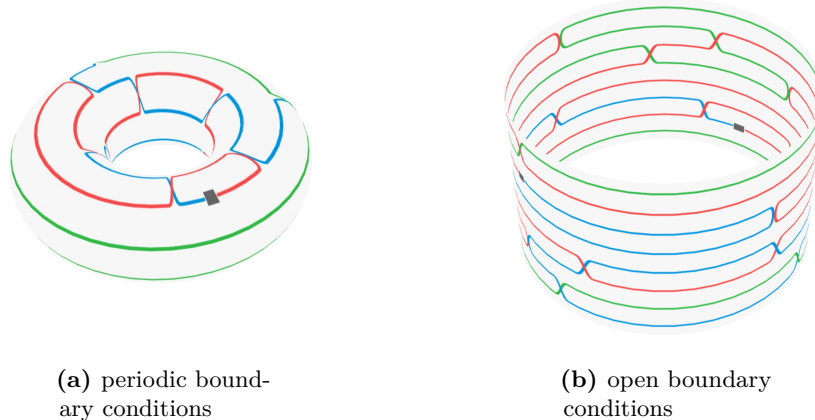


Figure 2.8. For the 3-color bosonic particle model, we consider both open and periodic boundary conditions as we will see in Chapter 3, there are some essential differences between (a) and (b).

The operator $e^{i\pi T^z}$ is diagonal in our basis, and its Eigenvalues are +1 for red and blue particles and -1 for green particles. To get the phase factor, we need to determine whether a configuration has an odd or even number of green particles between sites i and j. In principle, we would need to evaluate the occupancy at all

sites k between i and j and at every time. Fortunately, the types of interactions present in our model don't change the number of green particles from odd to even (or vice versa). The only way this number can change is when there are interactions that are linked to site i or j , i.e. a green particle enters or leaves the sites between head and tail. For the graphical representation in [Figure 2.8](#), this means we only need to know what is happening on the dashed line. At each measurement, we need to determine the occupation at $\tau = 0$. We look for interactions at the dashed line, which involves the colour green. At these interactions, the phase factor changes.

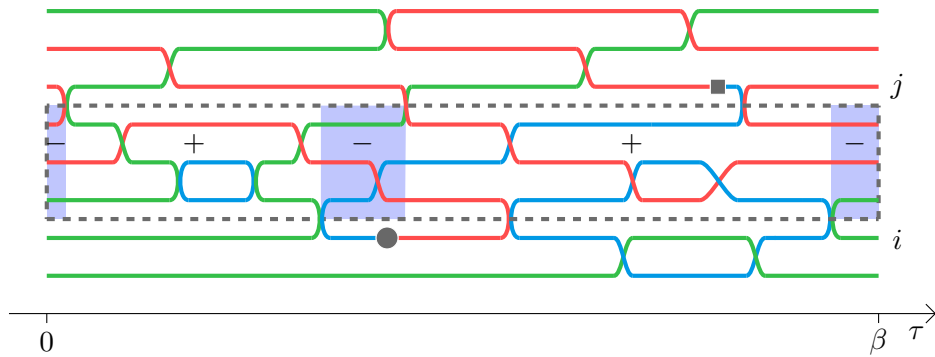


Figure 2.9. Graphical representation of an open-worldine configuration of the 3-color bosonic particle model. The Spin-Spin correlation function is evaluated when the head and tail are at equal times in the Greens function sector.

Chapter 3

The AKLT Model and Matrix Product States

3.1 Haldane's Conjecture

The spin- $\frac{1}{2}$ antiferromagnetic Heisenberg chain can be solved exactly by a so-called Bethe Ansatz. Hans Bethe developed this method in the 1930s [32]. The ground state of this model has the following properties.

1. The ground state is unique, no symmetries are spontaneously broken
2. Excitations are "massless", meaning that the gap ΔE between the ground state and the first excited state vanishes in the thermodynamic limit. There is a continuum of states just above the ground state.
3. The spin-spin correlation function decays according to a power-law

At that time, no one seriously investigated the physics of the spin-1 antiferromagnetic Heisenberg chain or any higher spin case. The common belief was that the properties of this model are qualitatively the same as in the spin- $\frac{1}{2}$ case. However, in 1983 Duncan Haldane published a highly influential paper [33] in which he argued that the spin-1 model and, more generally, any integer spin chain has different properties, namely:

1. The ground state is unique, just as in the spin- $\frac{1}{2}$ case
2. Excitations are "massive", meaning a finite gap ΔE between the ground state and the first excited state even in the thermodynamic limit.
3. The spin-spin correlation function decays exponentially

This became known as the Haldane conjecture. The investigation of the Haldane phenomena influenced many new developments in low-dimensional quantum systems. Among which are new numerical techniques, most notably the Density-Matrix-Renormalization-group and Matrix Product states. They were introduced as an efficient representation of the states of quantum spin chains. Last but not least theoretical understanding of the Haldane phenomena in terms of symmetry-protected topological led to the development of a new field in condensed matter physics. This

chapter will first discuss entanglement as it plays a significant role in understanding the Haldane phenomena. Next, we will discuss MPS and use it to construct the ground state of the AKLT model. We will then discuss the Kennedy Tasaki transformation and the relation to the negative sign problem in Quantum Monte Carlo. The Kennedy-Tasaki transformation also plays a central role in understanding the Haldane phase as symmetry-protected topological order.

3.2 Entanglement, Area Laws, and Computational Complexity

We will start this chapter with a rather general introduction to entanglement. Entanglement is one of the phenomena already studied in the early days of quantum mechanics. It is essential for the understanding of the energy levels in the Helium atom. Still, the thought Experiment proposed by Einstein-Podolski and Rosen in 1935 [34] baffled physicists for decades. It involved measurements on two entangled photons which were spacially separated. It took until 1964 when John Bell finally gave a satisfying explanation of the EPR experiment [35]. Only then Physicists started to gain a deeper understanding of entanglement, and quantum information theory emerged. In condensed matter physics, the role of entanglement was unclear for even longer. The qualitative difference between the integer and half-integer Antiferromagnetic Heisenberg model is due to the latter's non-trivial entanglement structure. One-dimensional quantum spin systems showed to be particularly interesting from an entanglement point of view. Affleck Kennedy, Lieb, and Tasaki proposed a slightly modified model which included an additional biquadratic term. AKLT showed that the bilinear-biquadratic spin-1 model chain with $\alpha = \frac{1}{3}$ and $\gamma = 1$ has a ground state which can be constructed exactly but shares many of its properties with the case $\alpha = 0$ studied by Haldane. The role of entanglement becomes very clear from the construction of the AKLT state. We will discuss the ground state properties of this model in some detail. The ground state can be constructed as a Matrix product state. Unlike Quantum Monte Carlo, where we described states in terms of a thermal density Matrix ρ , we now restrict our discussion to pure states. Entanglement can also be studied for the more general case of mixed states, but that is much more difficult. There are many different ways to define entanglement in that case. See, for example, the book by Wilde [36]. It is sufficient to discuss pure states for our purpose, as we are interested in the ground states. The pure state of a quantum spin chain can be fully specified by a set of $(2S + 1)^n$ complex coefficients:

$$|\psi\rangle = \sum_{\sigma_1, \dots, \sigma_n} c_{\sigma_1, \dots, \sigma_n} |\boldsymbol{\sigma}\rangle \quad (3.1)$$

In classical physics the number of coefficients scales linearly with system size. There is a subclass of pure states namely the product states, which also have this property:

$$|\psi\rangle = |\psi_1\rangle_1 \otimes |\psi_2\rangle_2 \otimes \cdots \otimes |\psi_n\rangle_n$$

with $|\psi_i\rangle_i = \sum_{j=1}^{2S+1} \alpha_{ij} |j\rangle_i$

(3.2)

Where $\{|1\rangle_i, \dots, |2S+1\rangle_i\}$ is the local basis on-site i . The product state is fully specified by a set of $n(2S+1)$ complex coefficients. Due to the normalization condition and an overall phase factor, the number of coefficients is actually less. But what is important is linear scaling. Product states which are not entangled, the definition for entanglement is straightforward: *A pure state is entangled if and only if it is not a product state.* Therefore, the need for exponential resources can be seen as a consequence of entanglement.

Let us consider a quantum system consisting of a part A and a part B. We can think of an n-site quantum spin chain with open boundary conditions for concreteness. We now cut to the right of a site m , with $1 < m < n$. We assign the sites $i \leq m$ to subsystem A and the sites $i > m$ to subsystem B. A basis for subsystem A is given by: $|0\rangle_A \in \{|1\rangle_A, \dots, |(2S+1)^m\rangle_A\}$. Equivalently for subsystem B: $|0\rangle_B \in \{|1\rangle_B, \dots, |(2S+1)^{n-m}\rangle_B\}$. A state $|\psi\rangle$ of the full system can be expressed as a sum of tensor products of the basis states:

$$|\psi\rangle = \sum_{k=1}^{(2S+1)^m} \sum_{l=1}^{(2S+1)^{m-n}} c_{kl} |k\rangle_A \otimes |l\rangle_B \quad (3.3)$$

The state is now fully specified by the $(2S+1)^m \times (2S+1)^{m-n}$ Matrix c_{kl} . For any Matrix we can define the singular value decomposition [37] :

$$c_{kl} = \sum_{i=1}^d U_{ki} D_{ii} V_{il}, \quad \text{with } d = \min((2S+1)^m, (2S+1)^{m-n}) \quad (3.4)$$

The Matrices U and V are left and right unitary respectively and therefore define a basis transformation. We define new bases for System A and B:

$$\tilde{i}\rangle_A = \sum_{k=1}^d U_{ki} |k\rangle_A, \quad |\tilde{j}\rangle_B = \sum_{l=1}^d V_{jl} |l\rangle_B \quad (3.5)$$

The Matrix D is a diagonal Matrix with real and non negative entries: $D_{ii} = \lambda_i > 0$. We can express the state $|\psi\rangle$ through our newly defined bases for System A and B. This form is known as the Schmidt decomposition:

$$|\psi\rangle = \sum_{i=1}^d \lambda_i |\tilde{i}\rangle_A \otimes |\tilde{i}\rangle_B \quad (3.6)$$

The λ'_i s are called Schmidt coefficients, and the number of non-zero Schmidt coefficients is the Schmidt rank r . The Schmidt rank tells us something about the bipartite entanglement of Subsystems A and B. A product state has a Schmidt rank of 1; the two subsystems are not entangled. The other limiting case is a maximally entangled state: *A state is maximally entangled iff the Schmidt rank is $r = d$ and Schmidt the coefficients $\lambda_i = \frac{1}{\sqrt{d}}$ for all $i \in \{1, \dots, d\}$.* We can now define entanglement Entropy, a measure for the entanglement of pure states:

$$S_{AB} = - \sum_{i=1}^d \lambda_i^2 \log(\lambda_i^2) \quad (3.7)$$

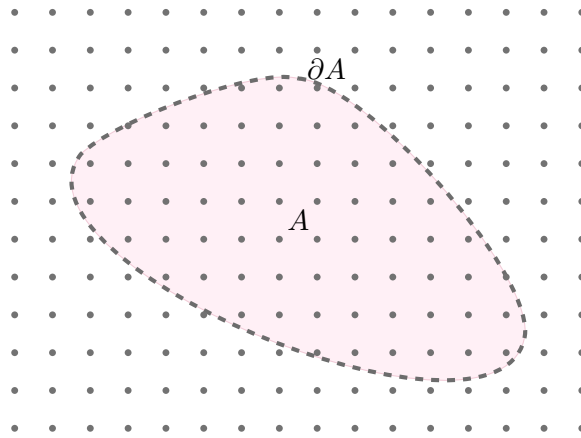


Figure 3.1. The name area law is used in any dimension even though the boundary is not an area.

From this definition, it is clear why we speak of entanglement between two subsystems, A and B. Still, we often find the notation S_A or S_B for S_{AB} . Now we focus specifically on the ground states of Hamiltonians. The Hamiltonians we are typically interested in have short-range interactions. In path Integral Monte Carlo, we restricted the discussion to Hamiltonians with nearest-neighbour interaction. There are many arguments why one would expect that entanglement for these classes of ground states is limited. It was conjecture that the ground states for local gapped Hamiltonians satisfy a so-called area law. For a general quantum state, the entanglement entropy is an extensive quantity. For a state satisfying an area law, the entanglement entropy only scales as the size of the boundary between two Subsystems. This boundary is an area in three dimensions, hence the name area law. Hastings found a rigorous proof for this conjecture for local gapped Hamiltonians in 1 dimension [38]. Suppose we go back to the case where we cut a chain with open boundary conditions of length N at $m = \frac{N}{2}$. If we consider the ground state of a local gapped Hamiltonian, then the entanglement Entropy is independent of N . For quantum critical regimes, the area law needs a logarithmic correction. The entanglement Entropy scales as $\log(N)$ [39]. Due to the area law, we don't need exponential resources to specify the ground state. Landau et al. [40] showed that one could find the ground state using a poly(n) algorithm. The computational complexity we mentioned in Chapter 1 intro is solved for a large class of 1d quantum spin systems. These findings suggest that the ground states of local gapped Hamiltonians are very special and that we can use Methods that do not work for generic Hamiltonians.

3.3 Matrix Product States

Next, we will look at Matrix product states which allows one to exploit the fact that the state obeys an area law. We follow [41] who introduced the notion of a Matrix product state in its modern form. The MPS is constructed iteratively using a sequence of Schmidt decompositions. We consider a general spin S chain with open boundary conditions. We start at one end of the chain, performing a Schmidt

decomposition. System A is just the first site, and system B is the rest of the spin chain. We get basis transformation from the local computational basis to a new basis $|\alpha_1\rangle_1 = \Gamma_{\alpha_1}^{[1]\sigma_1} |\sigma_1\rangle_1$, just as in (3.5) with the difference that the summation is implicit. We also get the $(2S+1)$ Schmidt coefficients $\lambda_{\alpha_1}^{[1]}$. The procedure is then iterated for the whole chain. One can rewrite the coefficients (3.1) for a general pure state as:

$$c_{\sigma_1, \dots, \sigma_n} = \sum_{\alpha_1, \dots, \alpha_{n-1}} \Gamma_{\alpha_1}^{[1]\sigma_1} \lambda_{\alpha_1}^{[1]} \Gamma_{\alpha_1 \alpha_2}^{[2]\sigma_2} \lambda_{\alpha_2}^{[2]} \cdots \Gamma_{\alpha_{n-1}}^{[n]\sigma_n} \quad (3.8)$$

Until now we have not used the fact that we are dealing with states which are only slightly entangled to use the phrasing of Vidal et al. (3.8). The number of Schmidt coefficients grows exponentially from left to right: $\dim(\alpha_i) = (2S+1)^i$. For states with limited entanglement the Schmidt rank is bounded by a value d which is independent of n : $r_i < d < \dim(\alpha_i)$ for all $i \in \{1, n\}$. The ground states of quantum spin chains satisfy this condition or are at least well approximated by reasonably small d . A bounded Schmidt rank implies an area law, we will see this with a concrete example. Before we do so, we bring (3.8) into a more compact form by combining $\Gamma_{\alpha_{l-1}\alpha_l}^{[l]\sigma_l} \lambda_{\alpha_l}^{[l]}$ to a single tensor $A_{\alpha_{l-1}\alpha_l}^{[l]\sigma_l}$. Now assuming that the Schmidt rank is bounded by d , a tensor $A_{\alpha_{l-1}\alpha_l}^{[l]\sigma_l}$ has $d \times d \times (2S+1)$ entries. We have $n-1$ tensors, so the number of coefficients we have to specify scales linearly with the chain length. We arrive at the MPS representation:

$$c_{\sigma_1, \dots, \sigma_n} = \sum_{\alpha_1, \dots, \alpha_{n-1}} A_{\alpha_1}^{[1]\sigma_1} A_{\alpha_1 \alpha_2}^{[2]\sigma_2} \cdots A_{\alpha_{l-1} \alpha_l}^{[l]\sigma_l} \cdots A_{\alpha_{n-1}}^{[n]\sigma_n} \quad (3.9)$$

If one wants to get the coefficient $c_{\sigma_1, \dots, \sigma_n}$ to express a state $|\psi\rangle$ in the computational basis one has to evaluate a n -fold Matrix product: $A^{[1]\sigma_1} A^{[2]\sigma_2} \cdots A^{[n-1]\sigma_{n-1}} A^{[n]\sigma_n}$ hence the name Matrix product state. We will now look at a very simple MPS. We don't consider the case $d=1$ as this is a product state with no entanglement. So the smallest non trivial value is $d=2$. It turns out that the AKLT state is a Matrix product state with $d=2$. AKLT did not formulate it as a Matrix product state, but in retrospect this is the most natural way to express the AKLT state.

3.4 The AKLT Model

Affleck, Kennedy Lieb, and Tasaki showed that they could obtain an exactly solvable model by adding a biquadratic term to the antiferromagnetic spin-1 Heisenberg chain. Thus, we now have a closer look at the antiferromagnetic interaction in the spin-1 Heisenberg chain.

$$H_{AFM} = \sum_{i=1}^N \mathcal{H}_{i,i+1} = \sum_{i=1}^N \mathbf{S}_i \cdot \mathbf{S}_{i+1} \quad (3.10)$$

Let's consider a single term $\mathbf{S}_i \cdot \mathbf{S}_{i+1}$ acting on two neighbouring spins. We make the following observations: In the lowest Energy, the two spins couple to total spin 0. The highest Energy level has a total spin 2, and there is the spin-1 level in between. The spin-1 level is lowered relative to the other levels when adding the biquadratic term. For a special value of the biquadratic coupling constant, the spin-1 and spin 0

levels become degenerate. This happens at $\alpha = \frac{1}{3}$. The Hamiltonian $H_{i,i+1}$ acts as a projector on the spin-2 subspace. To be a true projector, the AKLT Hamiltonian contains an additional prefactor and a constant Energy shift. This does not change the Eigenstates of the Hamiltonian:

$$H_{AKLT} = \sum_{i=1}^N \left[\frac{1}{2} \mathbf{S}_i \cdot \mathbf{S}_{i+1} + \frac{1}{6} (\mathbf{S}_i \cdot \mathbf{S}_{i+1})^2 + \frac{1}{3} \right] = \sum_{i=1}^N P_2(\mathbf{S}_i + \mathbf{S}_{i+1}) \quad (3.11)$$

It is easy to verify that $P_2(\mathbf{S}_i + \mathbf{S}_{i+1}) = [P_2(\mathbf{S}_i + \mathbf{S}_{i+1})]^2$ using the explicit Matrix representation. What might be surprising is that the full Hamiltonian consisting of a sum of projectors still has a zero Energy Eigenstate. This state is constructed as follows:

1. Two spin- $\frac{1}{2}$ are coupled to a triplet state which can be associated with physical spin-1 degree of freedom at each site.
2. Each spin- $\frac{1}{2}$ is coupled to a singlet with a neighbouring spin- $\frac{1}{2}$

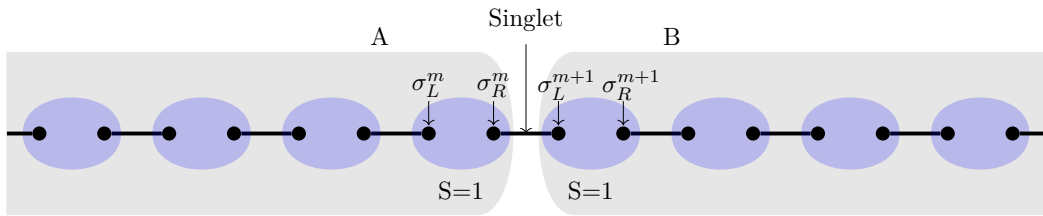


Figure 3.2. Visual representation of the valence bond state.

(2) ensures that the total spin of two neighbouring spin-1s can not be 2. We can relate this to the previous chapter. The singlet state is the maximally entangled state of two spin- $\frac{1}{2}$'s. If we cut the spin chain at any bond, the AKLT state has the form

$$|\psi_{AKLT}\rangle = \frac{1}{\sqrt{2}} |\psi_\uparrow\rangle_A \otimes |\psi_\downarrow\rangle_B - \frac{1}{\sqrt{2}} |\psi_\downarrow\rangle_A \otimes |\psi_\uparrow\rangle_B \quad (3.12)$$

$|\psi_\downarrow\rangle_A$ is a shorthand notation for the state of the Subsystem where the spin σ_R^m is in the down state, see Figure 3.2. From (3.12) we also find that the Schmidt rank is 2 and the entanglement entropy carried by a bond is $S = 2[\frac{1}{2} \ln(\frac{1}{2})]$ independent of the chain length. This means that the AKLT state satisfies the area law, and it can be expressed as an MPS with bond dimension 2. We further notice that this construction results in a translationally invariant state. Thus we have $A^{[l]} = A$ for the MPS representation(3.9). We now closely follow [11]. To find A, we first define a Matrix Σ , which incorporates the fact that the spins form a singlet:

$$\Sigma = \begin{vmatrix} |\uparrow\rangle_R^m & |\downarrow\rangle_R^m \end{vmatrix} \begin{pmatrix} \langle \uparrow |_L^{m+1} & \langle \downarrow |_L^{m+1} \\ 0 & \frac{1}{\sqrt{2}} \\ -\frac{1}{\sqrt{2}} & 0 \end{pmatrix} \quad (3.13)$$

Next one defines a tensor M which maps the two local spin- $\frac{1}{2}$ onto the physical spin-1 degree of freedom. The matrices contain the three symmetric combinations:

$$M^+ = \begin{array}{c} \langle \uparrow |_R^m \quad \langle \downarrow |_R^m \\ |\uparrow \rangle_L^m \quad |\downarrow \rangle_L^m \end{array} \left(\begin{array}{cc} 1 & 0 \\ 0 & 0 \end{array} \right) \quad M^0 = \begin{array}{c} \langle \uparrow |_R^m \quad \langle \downarrow |_R^m \\ |\uparrow \rangle_L^m \quad |\downarrow \rangle_L^m \end{array} \left(\begin{array}{cc} 0 & \frac{1}{\sqrt{2}} \\ \frac{1}{\sqrt{2}} & 0 \end{array} \right)$$

$$M^- = \begin{array}{c} \langle \uparrow |_R^m \quad \langle \downarrow |_R^m \\ |\uparrow \rangle_L^m \quad |\downarrow \rangle_L^m \end{array} \left(\begin{array}{cc} 0 & 0 \\ 0 & 1 \end{array} \right)$$

Finally, one combines the two tensors into single tensor A by summing over the σ_R^m index. After normalization, the Tensor A reads:

$$A^+ = \begin{pmatrix} 0 & \sqrt{\frac{2}{3}} \\ 0 & 0 \end{pmatrix} \quad A^0 = \begin{pmatrix} -\frac{1}{\sqrt{3}} & 0 \\ 0 & \frac{1}{\sqrt{3}} \end{pmatrix} \quad A^- = \begin{pmatrix} 0 & 0 \\ -\sqrt{\frac{2}{3}} & 0 \end{pmatrix} \quad (3.14)$$

We arrive at the Matrix product representation of the AKLT state:

$$|\psi_{AKLT}\rangle = \sum_{\sigma} \sum_{\alpha_1, \dots, \alpha_n} A_{\alpha_n \alpha_1}^{\sigma_1} A_{\alpha_1 \alpha_2}^{\sigma_2} \cdots A_{\alpha_{l-1} \alpha_l}^{\sigma_l} \cdots A_{\alpha_{n-1} \alpha_n}^{\sigma_n} |\sigma\rangle \quad (3.15)$$

Different from the previous definition of MPS,(3.9) we have used periodic boundary conditions. This is actually the simplest case, as all sites are treated on an equal footing. The first and the last tensor A carry a common index α_n . They also share a singlet bond, just like all the other sites. Affleck, Kennedy, Lieb, and Tasaki proved in a subsequent paper that the valence bond state is the unique ground state of the AKLT model. Furthermore, the concept of a valence bond state was extended to a 2-dimensional hexagonal lattice, for which it is also a unique ground state. This might not be very surprising from the construction, as we have no choice but to form singlets for the projection operator to yield zero. The rigorous proof is one of the important results which coincides with Haldane's predictions for the antiferromagnetic Heisenberg model. The AKLT state has a non-trivial entanglement structure, expressed in the computational basis it is a superposition of many basis states. To find a coefficient $c^{\sigma_1, \sigma_2, \dots, \sigma_{n-1}, \sigma_n}$ in the computational basis one has to evaluate a trace over an n-fold Matrix product $c^{\sigma_1, \sigma_2, \dots, \sigma_{n-1}, \sigma_n} = Tr(A^{\sigma_1} A^{\sigma_2} A^{\sigma_3} \cdots A^{\sigma_{n-1}} A^{\sigma_n})$. The A Matrices are proportional to spin- $\frac{1}{2}$ operators namely: $A^+ = \sqrt{\frac{2}{3}} S^+$, $A^- = -\sqrt{\frac{2}{3}} S^+$ and $A^0 = \sqrt{\frac{2}{3}} S^z$. Make the following observations:

1. The spin raising and lowering operators satisfy: $(S^\pm)^2 = 0$. Therefore, a spin raising operator must always be followed by a spin lowering operator. In between, there can be an arbitrary number of S^z operators. Only basis states of the form $|\dots 0 + 0 \dots 0 - 0 \dots 0 + -0 \dots\rangle$ which posses a sort of antiferromagnetic order have a non-vanishing coefficient. This is very different from standard antiferromagnetic order as we can have an arbitrary number of 0's in between the alternating spins.

2. The total number of (S^+) operators must equal the number of (S^-) operators. This condition is imposed by the trace. A state of the form $|0 + 0 \cdots 0 + - + 0\rangle$ would have vanishing weight as it has a $+$ both at the beginning and at the end of the sequence, again not considering the $0's$. As a consequence of this constraint, the AKLT state has $S^{tot} = 0$

The new type of order is one of the features of the AKLT state, which needs some deeper analysis. Another exotic feature is found when considering open boundary conditions.

3.5 Boundary Conditions and Free Edge Spins

Often boundary conditions are a minor subtlety when dealing with quantum spin chains, not so in the AKLT model. The proof of the uniqueness of the ground state by AKLT only holds for periodic boundary conditions. When we have open boundary conditions, the situation is different. Let us review the construction of the AKLT state. We started with forming singlets between neighbouring spin- $\frac{1}{2}$'s. With open boundary conditions, the sites at the Edge of the chain both have a spin- $\frac{1}{2}$ which does not have a neighbour to form a singlet. As a consequence, we have an effective spin- $\frac{1}{2}$ degree of freedom at the edges. The rest of the construction is equivalent to the case with open boundary conditions. The AKLT hamiltonian now has four zero Energy states: $|\psi_{AKLT}^{\uparrow\uparrow}\rangle, |\psi_{AKLT}^{\uparrow\downarrow}\rangle, |\psi_{AKLT}^{\downarrow\uparrow}\rangle, |\psi_{AKLT}^{\downarrow\downarrow}\rangle$. If we again look at the non-vanishing coefficients $c^{\sigma_1, \sigma_2, \dots, \sigma_{n-1}, \sigma_n}$ we observe that there are some differences to the previous case. Let us consider the state $|\psi_{AKLT}^{\uparrow\uparrow}\rangle$ in the valance bond picture. The left and right Edge spins are fixed to $|\uparrow\rangle$. This restricts the state of the spin-1 at the first and last site to either $|+\rangle$ or $|0\rangle$. If the state $|0\rangle$ is chosen, then the neighbouring spin is again restricted to either $|+\rangle$ or $|0\rangle$, see fig. In the same way, we can find the ground states contributing to the other three ground states. A state of the form $|0 + 0 \cdots 0 - +\rangle$ only contributes to the state $|\psi_{AKLT}^{\uparrow\uparrow}\rangle$, while a state $|0 + 0 \cdots + - 0\rangle$ only contributes to $|\psi_{AKLT}^{\downarrow\downarrow}\rangle$. The only exception is the basis state containing only $0's$ as it contributes to both $|\psi_{AKLT}^{\uparrow\uparrow}\rangle$ and $|\psi_{AKLT}^{\downarrow\downarrow}\rangle$. The states $|\psi_{AKLT}^{\uparrow\downarrow}\rangle$ and $|\psi_{AKLT}^{\downarrow\uparrow}\rangle$ are hence not orthogonal. Just like the ground state of the

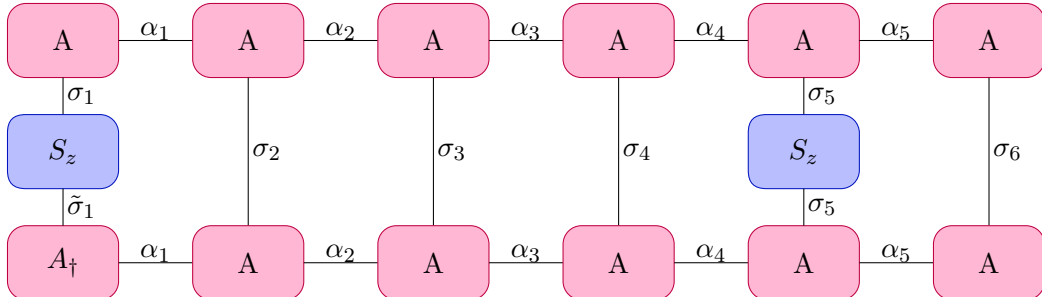


Figure 3.3. The Matrix product operator allows evaluation of the spin-spin correlation function.

periodic case they both have $S_{tot} = 0$. The basis states contributing to $|\psi_{AKLT}^{\uparrow\uparrow}\rangle$ and

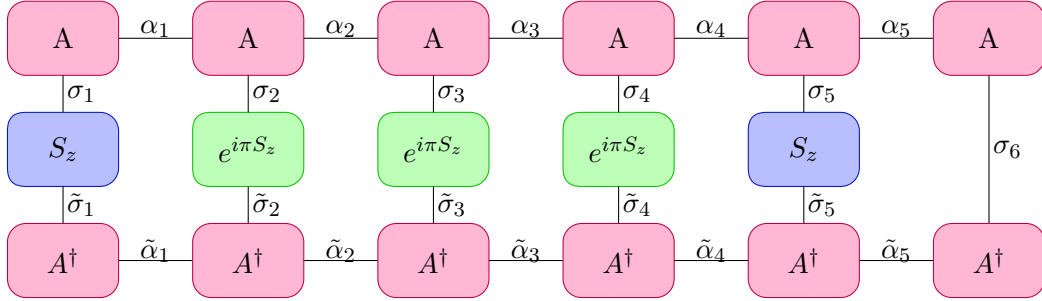


Figure 3.4. The Matrix product operator allows evaluation of the string correlation function.

$|\psi_{AKLT}^{\downarrow\downarrow}\rangle$ have $S_{tot} = 1$ and $S_{tot} = -1$. They are mutually orthogonal to the other ground states.

3.6 Spin-Spin and String Correlation functions

The MPS formalism allows us to construct the AKLT state explicitly and gives access to ground-state correlation functions. We can compare this with the Monte Carlo Results at finite temperature. To evaluate the correlation function, one needs to express operators in the MPS language. For a general introduction on this topic, we refer to section 4 of Schollwock [11]. In figure, we have a visual representation of the MPS construction for the spin-spin correlation function. For translationally invariant Matrix product states like the AKLT state, one can calculate correlation lengths explicitly, using the Transfer operator. The hidden antiferromagnetic order can be detected using the string order parameter. This non-local order parameter was introduced by Nijs et al. [42]. Most importantly, for our purpose, one can explicitly calculate the string order parameter. [11]:

$$O_{\text{String}}^a(\psi_{AKLT}) = \lim_{j-i \uparrow \infty} \lim_{L \uparrow \infty} \left\langle S_i^z e^{i\pi \sum_{i < k < j} S_k^z} S_j^z \right\rangle = \frac{4}{9} \quad (3.16)$$

Chapter 4

Phase Diagram

In this last chapter, we will compare the phase diagram of the bilinear biquadratic spin-1 chain obtained by our worm algorithm with the results of De Chiara et al. [9]. To do so, we will change the definition of the coupling constants to be in line with De Chiara et al. Instead of parameterizing the bilinear coupling constant with γ and α . We will use $\cos(\theta)$ and $\sin(\theta)$. This convention is most frequently used in the literature, as one can cover the whole parameter space of the anisotropic chain with just two parameters D and θ . The Hamiltonian reads:

$$H = \sum_{i=1}^{N-1} \cos(\theta) \vec{S}_i \otimes \vec{S}_{i+1} + \sin(\theta) (\vec{S}_i \otimes \vec{S}_{i+1})^2 + \sum_{i=1}^N D(S_i^z)^2 \quad (4.1)$$

One recovers the model studied by Affleck Kennedy Lieb and Tasaki [43] with $\theta = \arctan\left(\frac{1}{3}\right)$ and $D = 0$. It is interesting to consider the model with uniaxial anisotropy $D \neq 0$. This relatively simple model has a very rich phase diagram. Most

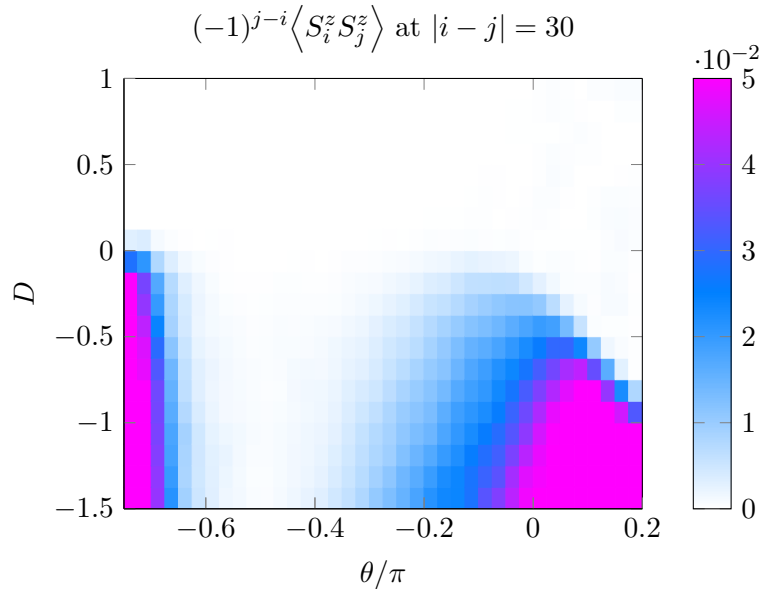


Figure 4.1. Contour plot of the spin order parameter for an open Chain with $N = 40$ and $\beta = 40$

phases are accessible using Monte Carlo Methods, even though we cannot find a negative-sign free representation for the full parameter space. It should also be noted that the uniaxial anisotropy does not affect the negative sign problem.

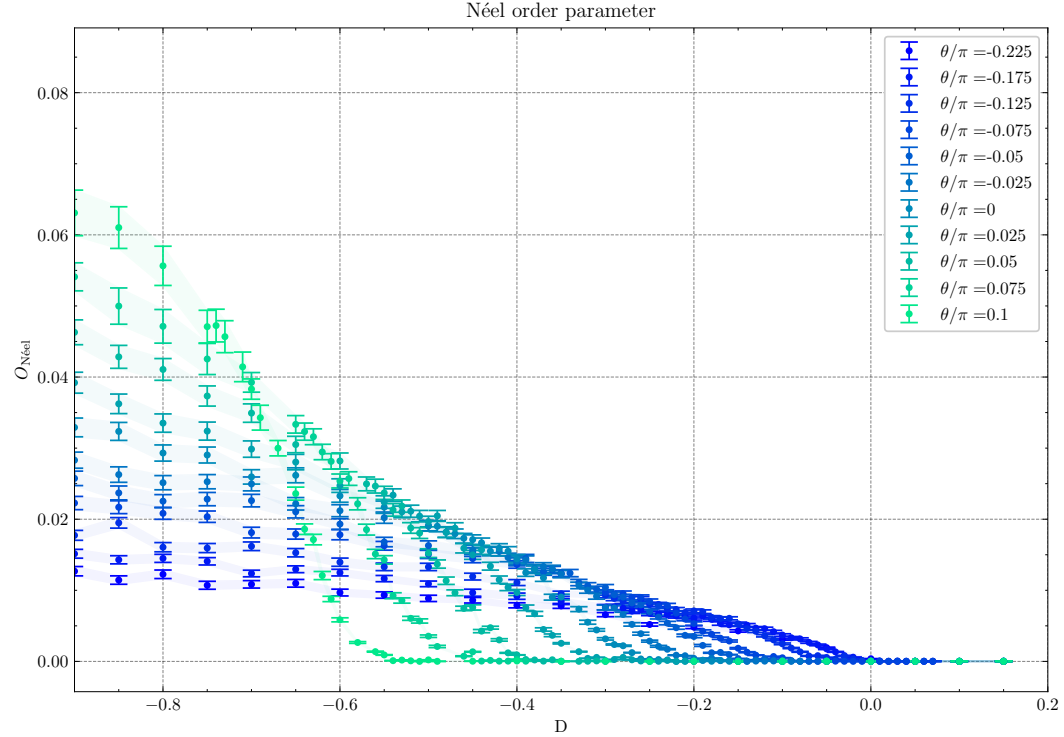


Figure 4.2. Néel order parameter from finite size data: $N = 80, \beta = 40$.

4.1 Large-D Phase

We will first briefly discuss the two limiting cases $D \rightarrow \infty$ and $D \rightarrow -\infty$. The easier of the two is the large- D limit, where we can neglect the bilinear and biquadratic terms:

$$H_{trivial} = \sum_{i=1}^N h_i = \sum_{i=1}^N D(S_i^z)^2 \quad (4.2)$$

This is a trivial example for a local gapped Hamiltonian. Assuming $D > 0$ the ground state of this Hamiltonian is readily found to be the product state:

$$\psi_{trivial} = |0\rangle_1 \otimes |0\rangle_2 \otimes \cdots \otimes |0\rangle_{n-1} \otimes |0\rangle_n \quad (4.3)$$

It is also easy to see that the Hamiltonian is gapped since an on-site excitation of the form $\cdots |0\rangle_{i-1} \otimes |+\rangle_i \otimes |0\rangle_{i+1} \cdots$ or equivalently $\cdots |0\rangle_{i-1} \otimes |-\rangle_i \otimes |0\rangle_{i+1} \cdots$ has Energy D . The model has a finite excitation gap $\delta E = D$ in the thermodynamic limit. This trivial Hamiltonian plays a key role in understanding the Haldane phase.

The limit of large negative D is more subtle; here, the ground state is not unique. The ground state pertains to the manifold spanned by [44]:

$$|\epsilon_1\rangle_1 \otimes |\epsilon_2\rangle_2 \otimes \cdots \otimes |\epsilon_{n-1}\rangle_{n-1} \otimes |\epsilon_n\rangle_n \quad (4.4)$$

where $\epsilon_i = \pm$. The model is effectively described by a spin- $\frac{1}{2}$ model. Different to the large-D limit, we have different phases depending on the choice of θ . These phases will be considered in the subsequent sections.

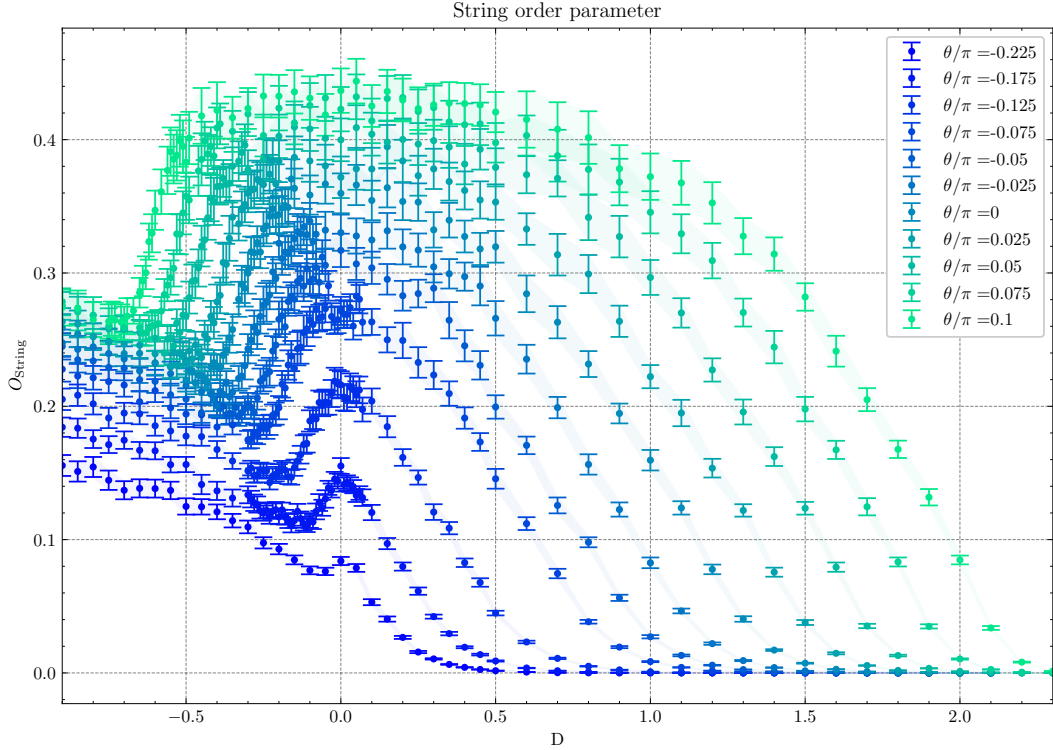


Figure 4.3. String Order parameter for a chain with periodic boundary conditions with $N = 80$ and $\beta = 40$.

4.2 Néel Phase

Condition (4.4) restricts the type of ordered phases we can expect for large negative D. Néel order is reported by [9] when a large negative D term is added to the AKLT model ($\theta = \arctan\left(\frac{1}{3}\right)$) as well as the antiferromagnetic Heisenberg model ($\theta = 0$). At the AKLT point any local correlation function decays exponentially [45], there is hence no Néel order. The Néel phase is characterized by a spontaneous staggered magnetization [9]. We can detect the Néel order by defining the following order parameter [45] :

$$O_{\text{N\'eel}}^a := \lim_{j \rightarrow i \uparrow \infty} \lim_{L \uparrow \infty} (-1)^{j-i} \langle S_i^a S_j^a \rangle_{\mathcal{H}} \quad (4.5)$$

In Section 2.6 we described a method to measure the spin-spin correlation function of the original system in the 3-color bosonic particle model. That was achieved by measuring phase factors in the open-worldline configuration. We can therefore estimate (4.5) in the 3-color bosonic particle model for $-0.5 < \frac{\theta}{\pi} < 0.25$. We obtain correlation functions for a range of parameters varying D and θ , see appendix A. We can confirm the findings of Okunishi et al. that both open boundaries conditions and open boundary conditions[30] :

The negative-sign free Hamiltonian is derived under the open boundary condition due to the non-local transformations. However, we have in practice performed the simulations under the usual periodic boundary condition by neglecting the non-local interaction between the boundary sites of $i = 1$ and L . Of course, the directed loop algorithm also works for the open boundary system. We have confirmed that the results for the open boundary are consistent with those for the periodic boundary, which implies that the periodic boundary condition yields no undesirable effect on the QMC simulation.

To avoid confusion, we explicitly use the subscript \mathcal{H} and $\hat{\mathcal{H}}$ to distinguish between the original Hamiltonian and the transformed Hamiltonian. In (2.22) we have described how this quantity can be measured in the Greens function sector of the transformed Hamiltonian.

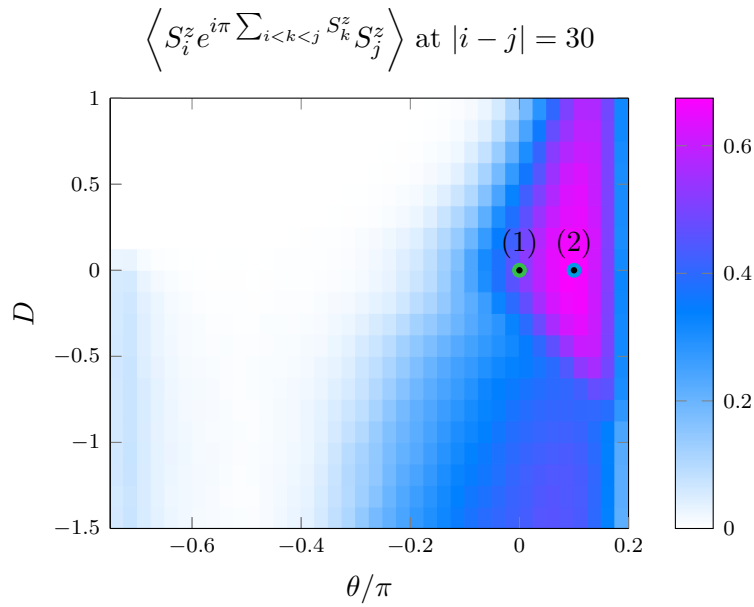


Figure 4.4. Contour plot of the string order parameter for an open Chain with $N = 40$ and $\beta = 40$. (1) is the antiferromagnetic Heisenberg model and (2) the AKLT model.

4.3 Haldane Phase

In Section 3.4 we observed that the AKLT ground state possesses a kind of order which is different from Néel order. Still, we observed some type of order that a local order parameter can not detect. It is often referred to as hidden antiferromagnetic

order. Hidden antiferromagnetic is present at the AKLT point and at the Heisenberg point, and the surrounding region for small positive and negative D. A non-local order parameter can be defined, called a string order parameter [42], to detect this type of order. Using the Kennedy Tasaki transformation, we map the string order to diagonal ferromagnetic order. We then map the string order to off-diagonal order with the R-Dimer basis. The off-diagonal correlation function can be estimated using the worm algorithm. We measure the string-order parameter in the region where the 3-color bosonic particle model is negative sign free see [Table 2.1](#) which corresponds to $-0.5\pi < \theta < 0.25\pi$ using the convention in [\(4.1\)](#). The string order parameter is defined as:

$$O_{\text{String}}^a := \lim_{j-i \uparrow \infty} \lim_{L \uparrow \infty} \left\langle S_i^a e^{i\pi \sum_{i < k < j} S_k^a} S_j^a \right\rangle_{\mathcal{H}} \quad (4.6)$$

The string order parameter has some special properties because of its non-local structure. The order parameter is non-zero not only for hidden antiferromagnetic order but also for usual ferrromagnetic order. Indeed the following property for the ground state holds [45] :

$$|O_{\text{N\'eel}}^a(\Phi_{\text{GS}})| \leq O_{\text{string}}^a(\Phi_{\text{GS}}) \quad (4.7)$$

Using this property, we can distinguish between the three phases: a N\'eel phase with antiferromagnetic order, the Haldane phase with hidden antiferromagnetic order and the large-D phase where both order parameters yield zero. It is easy to check that both [\(4.5\)](#) as well as [\(4.10\)](#) yield zero for the state [\(4.3\)](#). The three phases can be characterized by [22] :

$$\begin{array}{ll} \text{large- } D & O_{\text{N\'eel}}^a = O_{\text{string}}^a = 0 \text{ for } \alpha = 1, 2, 3 \\ \text{Haldane} & O_{\text{N\'eel}}^a = 0 \text{ for } \alpha = 1, 2, 3, O_{\text{string}}^1 = O_{\text{string}}^2 \neq 0, O_{\text{string}}^3 \neq 0 \\ \text{N\'eel} & O_{\text{string}}^3 \geq O_{\text{N\'eel}}^3 > 0, O_{\text{N\'eel}}^a = O_{\text{string}}^a = 0 \text{ for } \alpha = 1, 2 \end{array} \quad (4.8)$$

The hidden antiferromagnetic order is complete in the AKLT state. As a result, it was proved that the following property holds for any ground state [22]:

$$O_{\text{string}}^a(\Phi_{\text{GS}}) \leq O_{\text{string}}^a(\Psi_{\text{AKLT}}) = \frac{4}{9} \quad (4.9)$$

In [Figure 4.3](#) we plot the string order for a finite system size of $N = 80$ and $\beta = 40$. With this parameters we are essentially at the ground state expectation value of $\frac{4}{9}$ for the string order parameter near the AKLT point. In [appendix A](#) we include the correlation functions. Additionally we show a contour plot [Figure 4.4](#) for the string order parameter for open boundary conditions. We can confirm

4.4 Ferromagnetic Phase

Using the parametrization using θ , we find that the Hamiltonian is negative sign free in the parameter region $-\pi < \theta < -0.75\pi$. In this region, de Chiara et al. report a ferromagnetic phase which is diagonal in the S^z basis for $D < 0$. This can

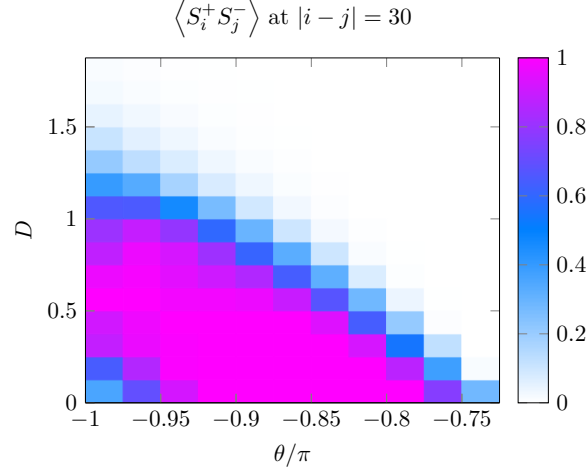


Figure 4.5. Planar order parameter for an open Chain with $N = 40$ and $\beta = 40$

be implemented by measuring the occupation number at a particular time slice in the partition function sector. Additionally, there is an XY-Ferromagnetic phase for small positive-D, with a phase transition to the large-D phase. Order expected in for small positive values of D is characterized by a diverging correlation function in the planar order parameter. The order parameter can be defined using the off-diagonal correlation function defined in (2.10):

$$O_{XY} := \lim_{j-i \uparrow \infty} \lim_{L \uparrow \infty} \langle S_i^+ S_j^- + S_i^- S_j^+ \rangle_{\mathcal{H}} \quad (4.10)$$

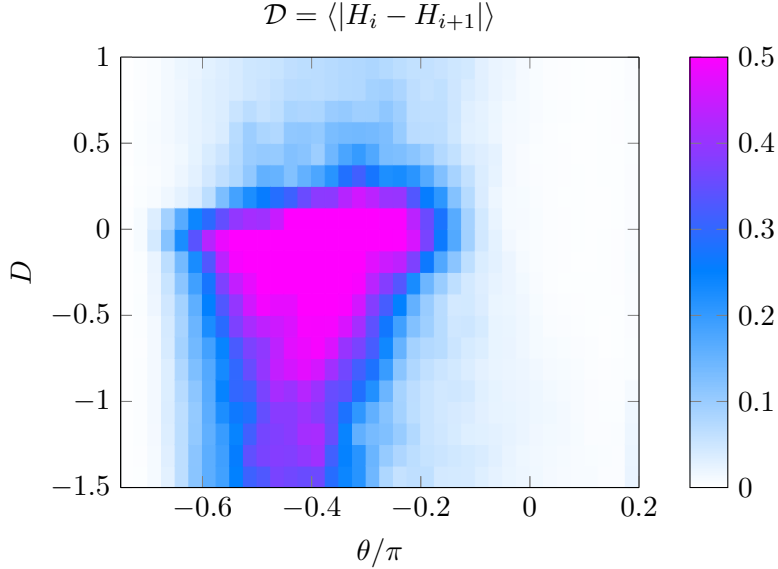


Figure 4.6. Dimer Order Parameter for an open Chain with $N = 40$ and $\beta = 40$

4.5 The Dimer Phase

In the Dimer phase, the translational invariance is broken due to the formation of singlets by neighbouring spins. We can detect this by measuring the Dimer order parameter. This quantity is diagonal in the computational basis, both in the original model and the 3-color bosonic particle model. We measure the Energy at each bond i individually and denote it by H_i . The measurement is performed by picking out a time slice in the closed path configuration. The dimer order parameter is defined [9] as:

$$\mathcal{D} = |H_i - H_{i+1}| \quad (4.11)$$

The dimer order parameter is predicted to be non-zero near $-\frac{\theta}{\pi} = 0.5$. Considering Table 2.1 one can find that we need to use different transformations $\frac{\theta}{\pi} > 0.5$ and for $\frac{\theta}{\pi} < 0.5$.

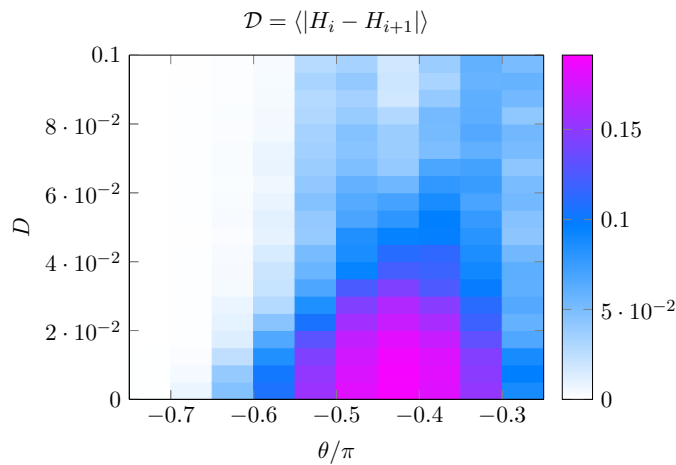


Figure 4.7. Dimer Order Parameter for an open Chain with $N = 40$ and $\beta = 40$.

We use the local transformation in the former, while the latter uses the non-local Kennedy-Tasaki transformation. Fortunately, the measurement of \mathcal{D} can be carried out in the same way as both models lead to the 3-color bosonic particle model. In Figure 4.6 we show the measurements for the Dimer order parameter in the entire parameter space covered by the 3-color bosonic particle model. The transition to the large- D phase occurs at $D < 0.1$. We, therefore, show this in a separate plot, see Figure 4.7.

4.6 Critical Phase

The parameter space, which can be simulated without a negative sign problem, also contains a critical phase predicted by [9]. It lies in the region $-0.75\pi < \theta < -0.5\pi$ where the local unitary transformation is used. We were although not able to investigate this phase in detail, as we are not able to measure the correlation function used by de Chiara et al.:

$$\mathcal{C}_{ij} = \left\langle S_i^x S_j^x \right\rangle_{\mathcal{H}} \quad (4.12)$$

We again use the subscript to denote the basis, in this case, the original system \mathcal{H} . We still measured correlation functions, although similar to the string correlation function, we used open-world line configurations in the 3-color bosonic particle model. As we are only using a local transformation in $-0.75\pi < \theta < -0.5\pi$ the correlation function does not sample string correlation function but a local quantity:

$$C_{ij} = \langle T_i^a T_j^a \rangle_{\hat{\mathcal{H}}} \quad (4.13)$$

In [Figure 4.8](#) we show a logarithmic plot of this correlation function at $\theta = -0.675\pi$ for different values of D . See [for](#) the correlation functions at different values of θ on a linear plot.

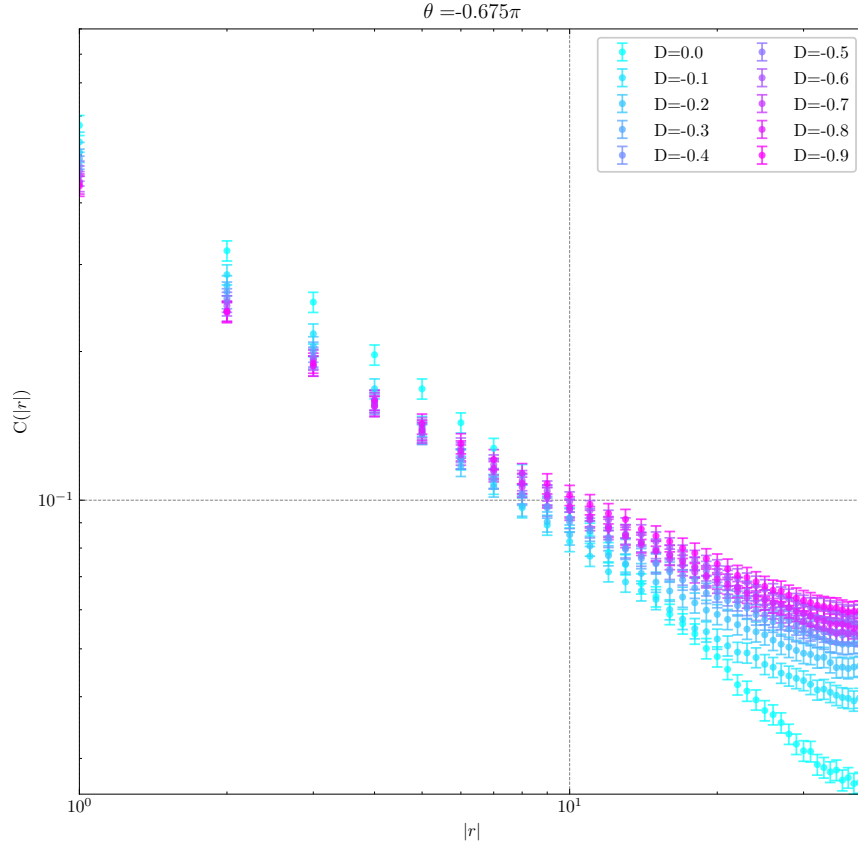


Figure 4.8. Logarithmic plot of the correlation function in the critical phase.

Chapter 5

Conclusion

In this thesis, we have studied the bilinear-biquadratic spin-1 model in the presence of an uniaxial anisotropy. We have developed a worm algorithm, which is a quantum Monte Carlo algorithm based on the path integral representation. The worm algorithm was invented in the 1990s by Prokovief et al [6]. It is one of the most popular methods to study bosonic lattice models and spin systems. Many spin models suffer from the so-called negative sign problem, which causes an exponential increase in computation time. This problem is present when the Hamiltonian has non-positive off-diagonal elements. In principle, removing the negative sign problem is always possible by an appropriate basis transformation. In practice, it is often impossible to find such a transformation. This problem is known to be NP-hard [7].

In Chapter 2 we have discussed the development of a negative-sign free algorithm for the bilinear biquadratic spin-1 model. We extended the original formulation of the worm algorithm, which doesn't include biquadratic interactions. We found that the sign problem depends on the choice for the bilinear and biquadratic coupling constants. There are several known transformations that can cure the negative sign problem. Among them are the Kennedy-Tasaki transformation and various local transformations. The Kennedy-Tasaki transformation can remove the negative sign problem at the AKLT point [30]. The AKLT point is a special point where the ratio between bilinear and biquadratic constant is 3 [46]. Still, we could not solve the negative-sign problem in all cases. Recent studies suggest that the sign problem can be mitigated in some instances [47], this was not further investigated.

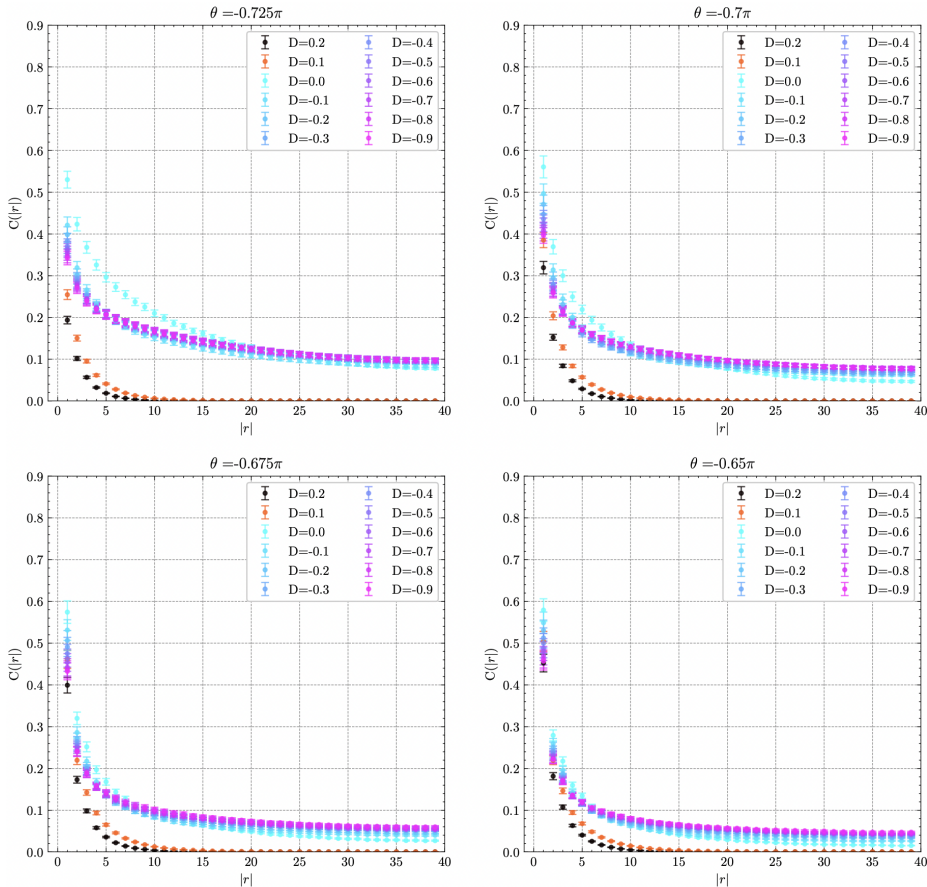
In Chapter 3, we have discussed the AKLT model in more detail using Matrix-Product-States (MPS). MPS can be used to investigate the entire parameter space of the bilinear biquadratic spin-1 model. At the AKLT point, it is possible to construct the ground state explicitly [11]. This is possible due to the particular entanglement structure of the ground state. In fact, this is closely related to the Kennedy-Tasaki transformation. The Kennedy-Tasaki transformation not only cures the negative-sign problem but also disentangles the AKLT ground state [30].

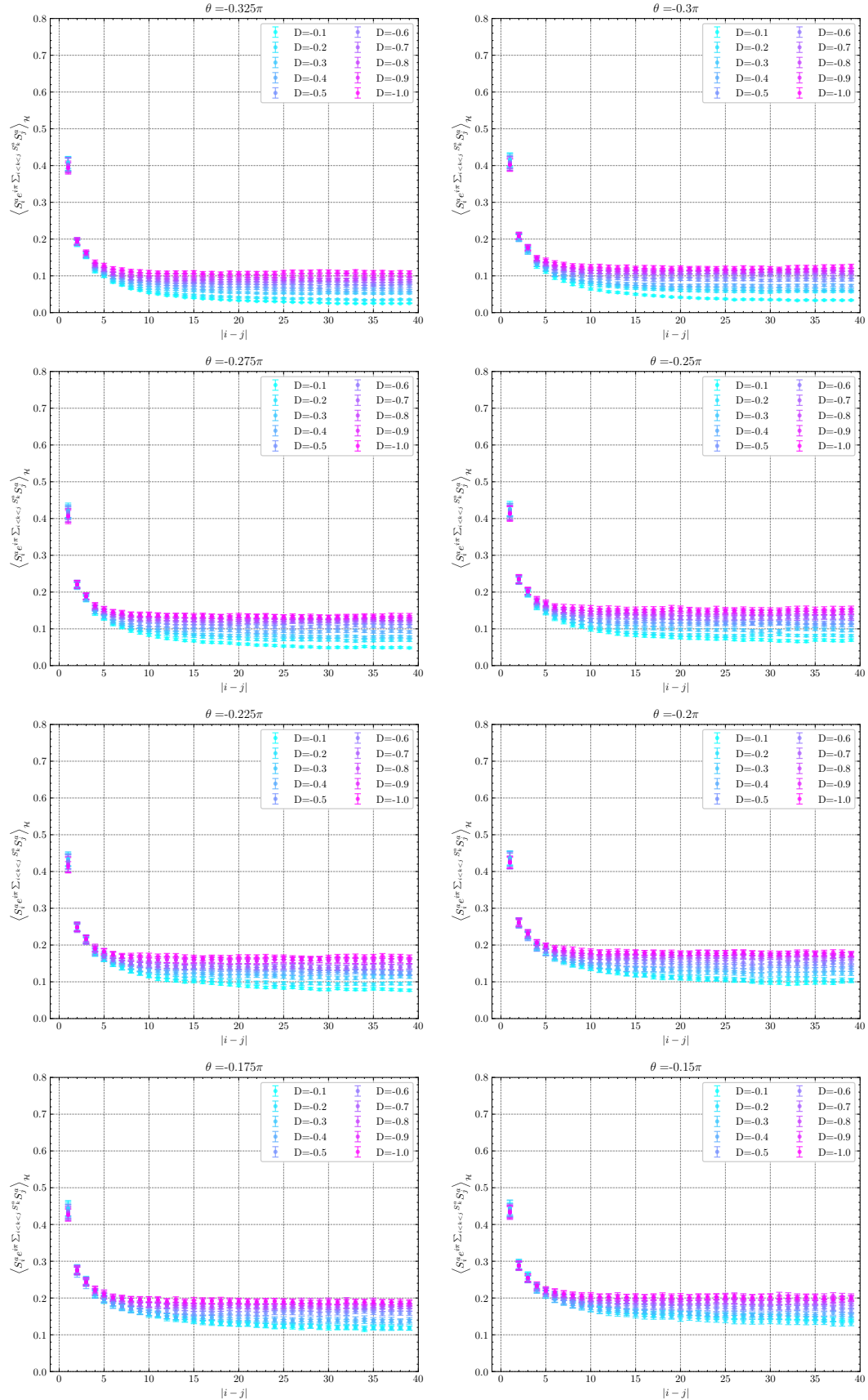
In Chapter 4 we discussed the phase diagram of the bilinear biquadratic spin-1 model. Our implementation of the worm algorithm gives us access to various order parameters. Among them is the string order parameter, which characterizes the order found in the AKLT model. Besides the string order, we investigate the rich phase diagram of the bilinear-biquadratic spin-1 model. We discuss dimerized, ferromagnetic, and antiferromagnetic phases, all accessible to the negative-sign free worm algorithm.

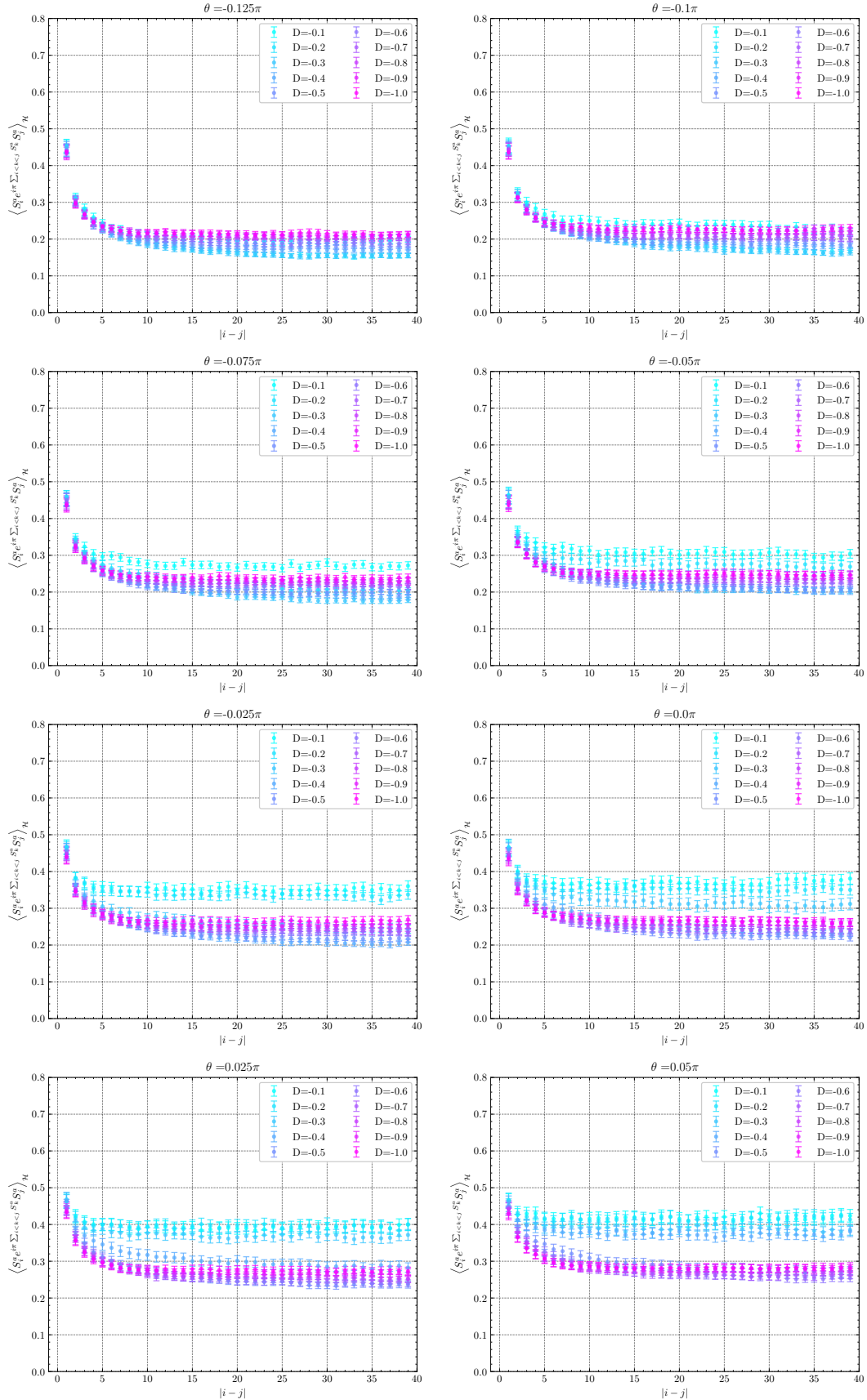
Appendix A

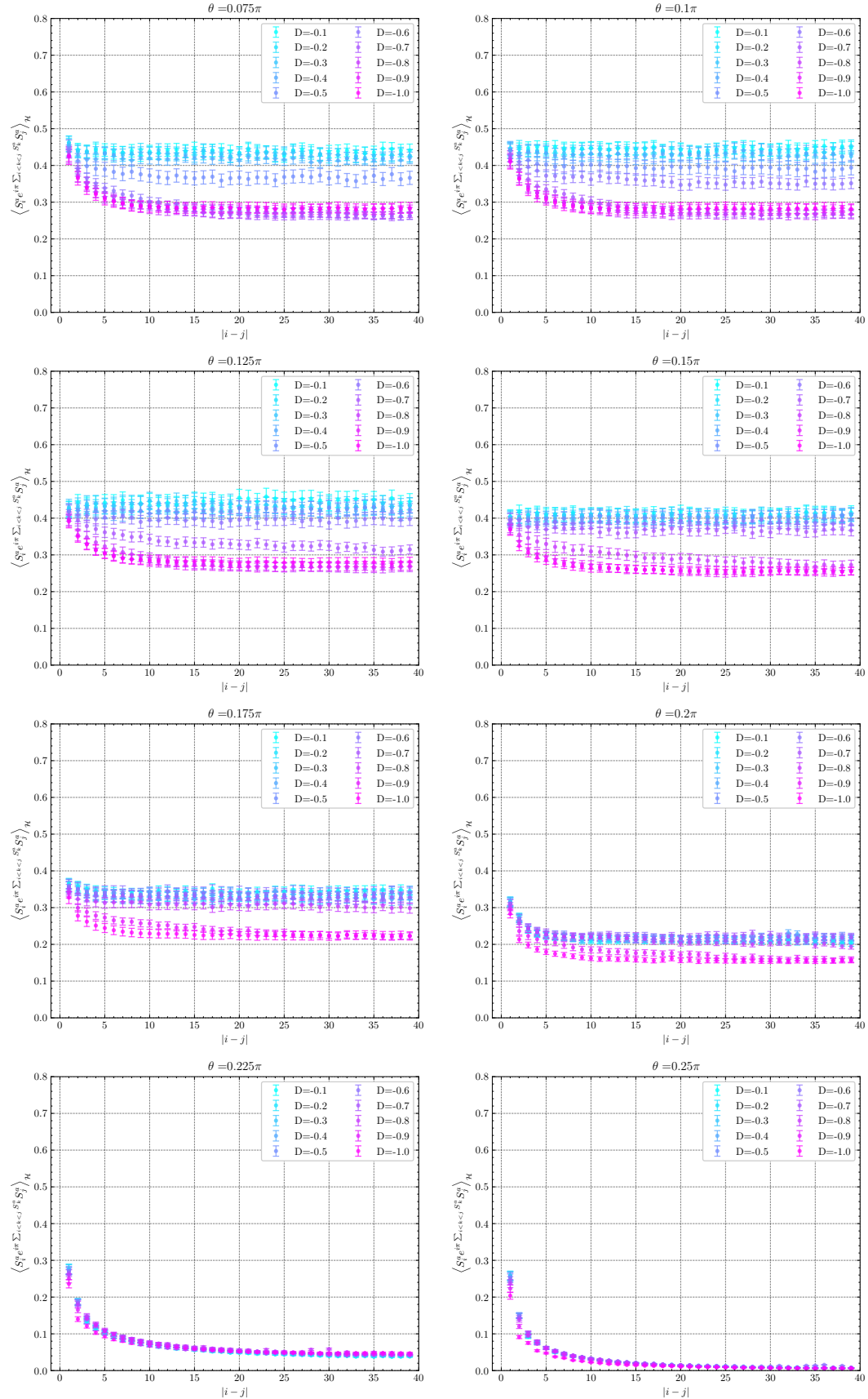
Correlation Functions

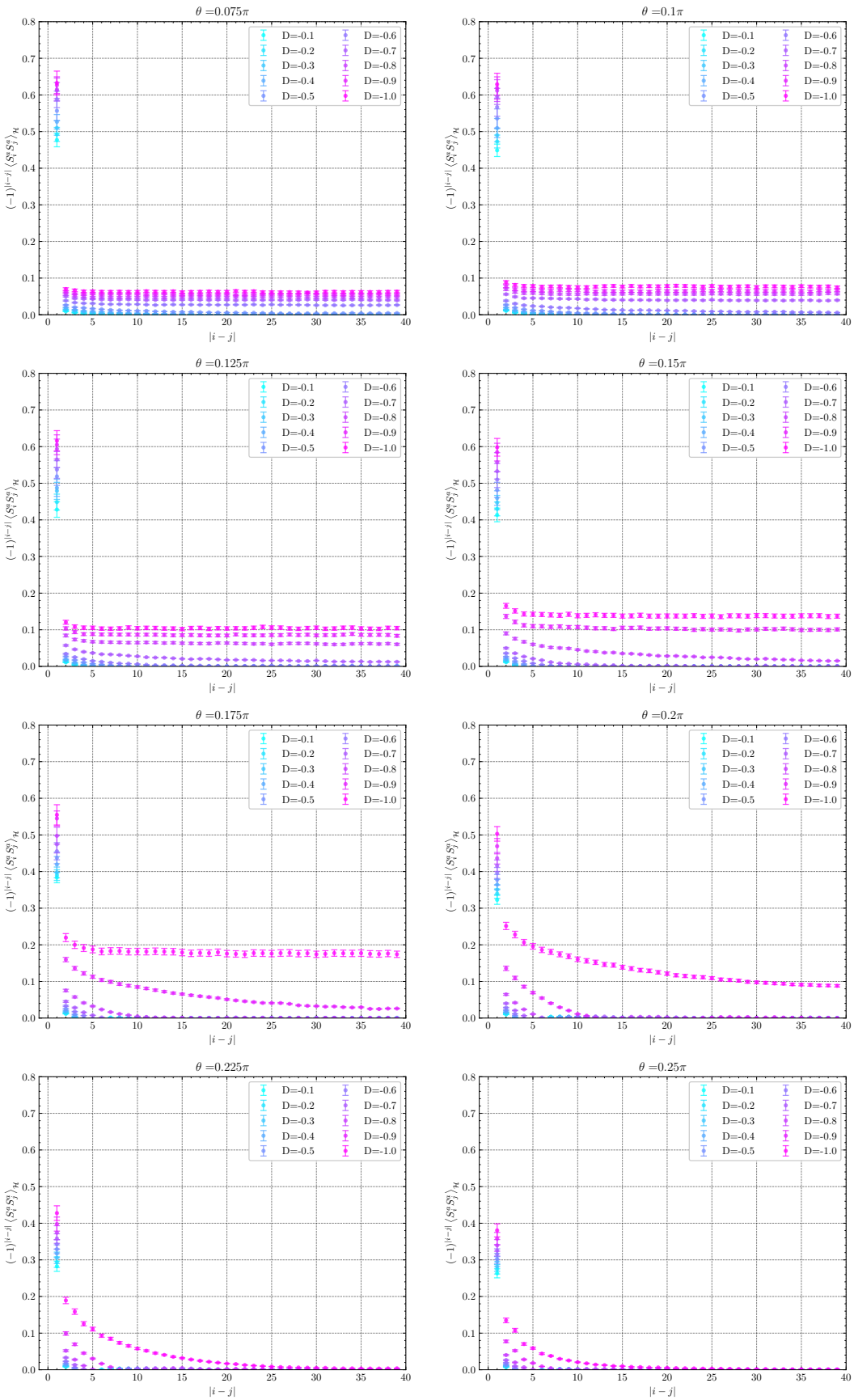
The following correlation functions were obtained from a chain with $N = 80$ at $\beta = 40$ and with periodic boundary conditions. The featured correlation functions are: off-diagonal correlation function in the critical phase (Page 55), string correlation function for negative D (Pages 56-58), spin-spin correlation function for positive D (Page 59), string correlation function for positive D (Pages 60-62). 0

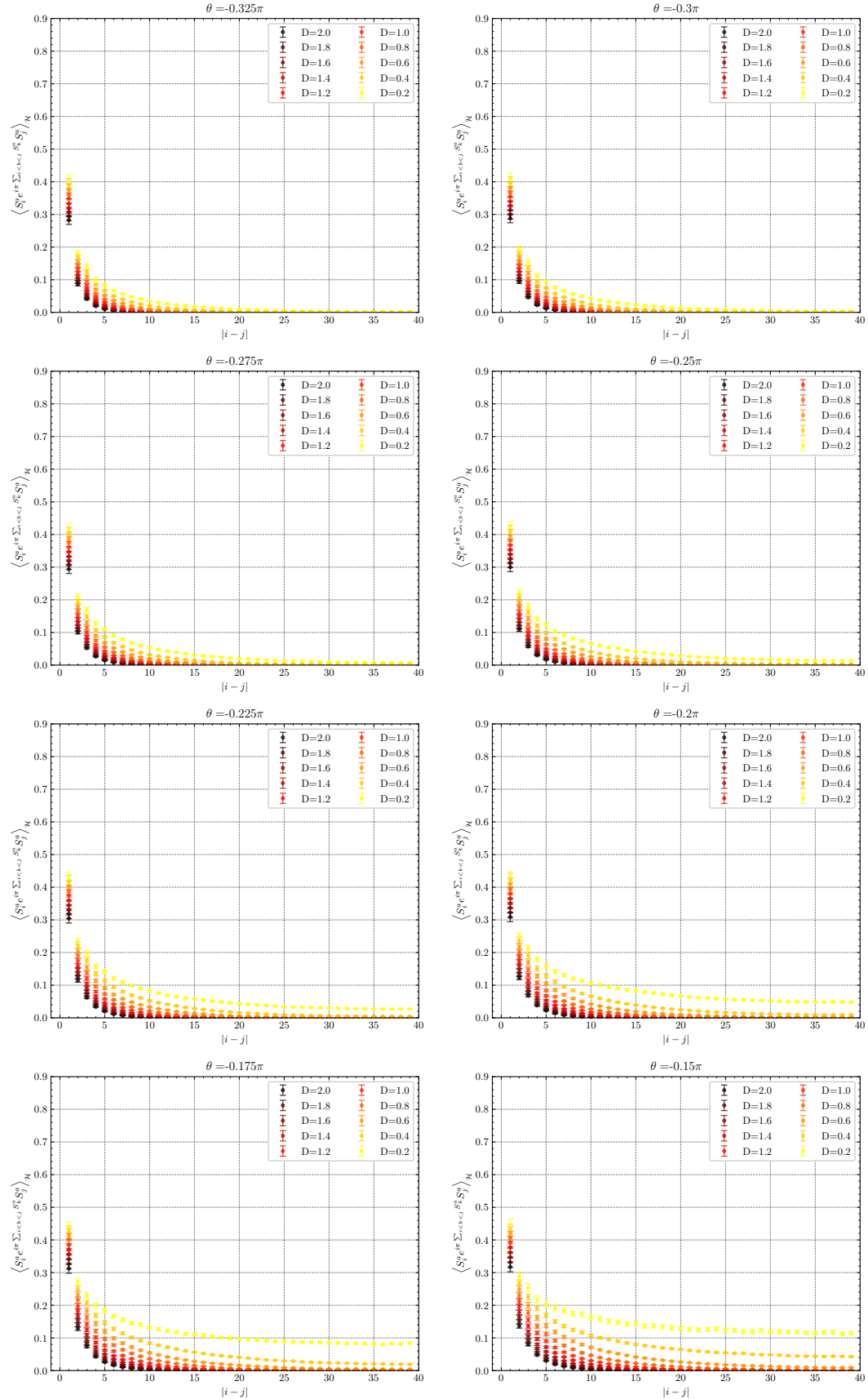


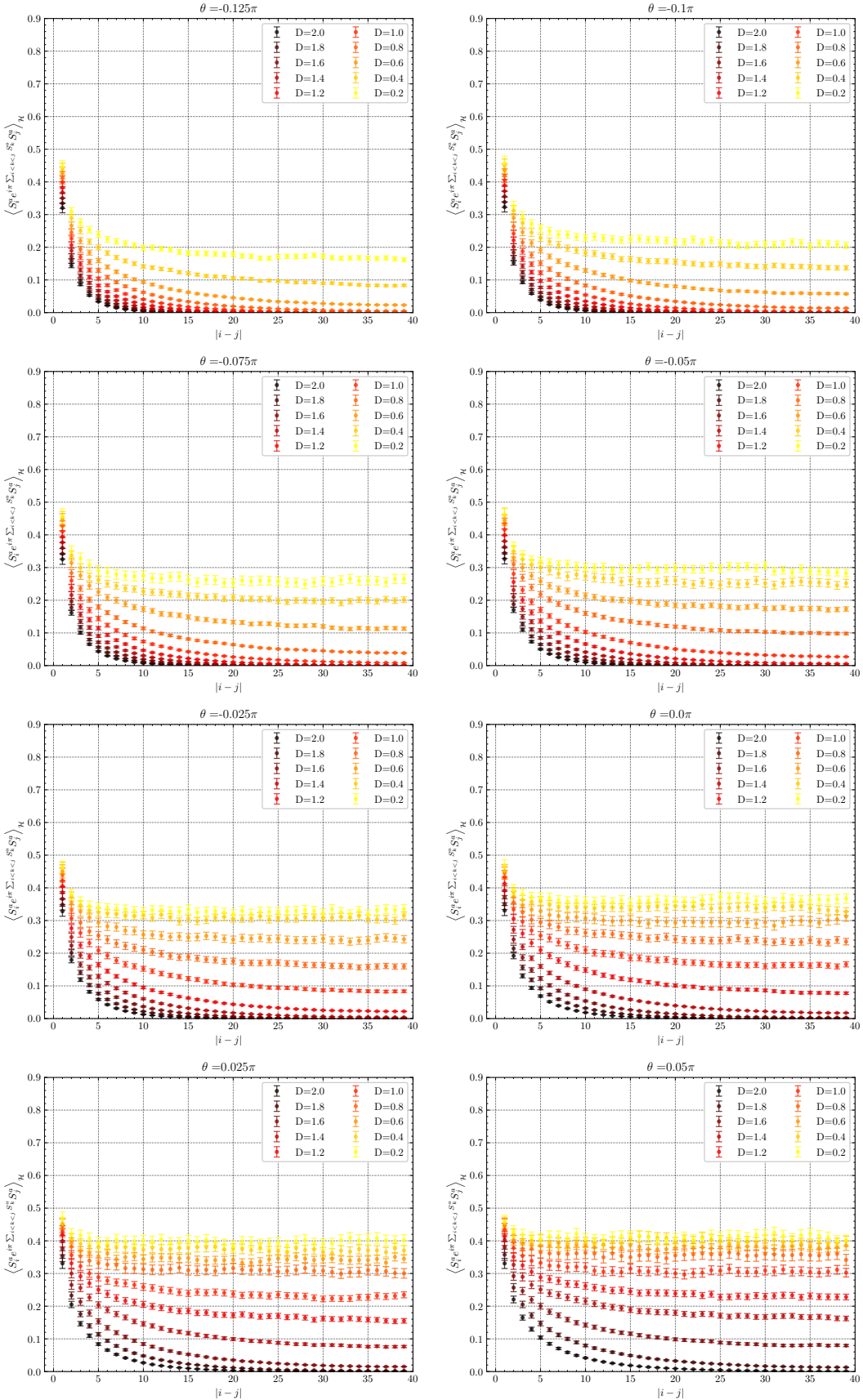


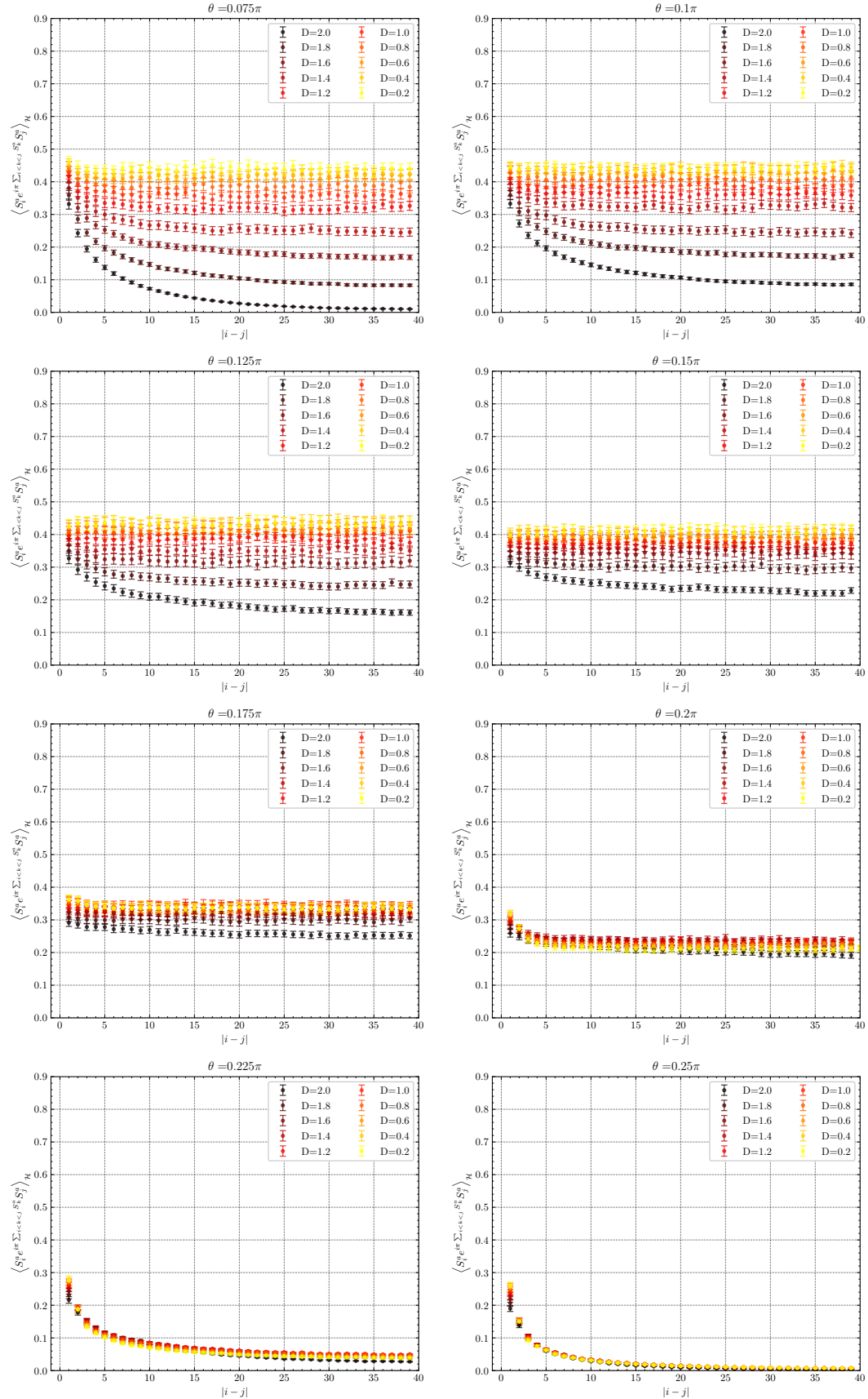












Bibliography

- [1] F. D. M. Haldane. Nonlinear Field Theory of Large-Spin Heisenberg Antiferromagnets: Semiclassically Quantized Solitons of the One-Dimensional Easy-Axis N\'eel State. *Physical Review Letters*, 50(15):1153–1156, April 1983. Publisher: American Physical Society.
- [2] I. Affleck. Quantum spin chains and the Haldane gap. *Journal of Physics: Condensed Matter*, 1(19):3047–3072, May 1989. Publisher: IOP Publishing.
- [3] Ian Affleck, Tom Kennedy, Elliott H. Lieb, and Hal Tasaki. Rigorous results on valence-bond ground states in antiferromagnets. *Physical Review Letters*, 59(7):799–802, August 1987. Publisher: American Physical Society.
- [4] Frank Pollmann, Erez Berg, Ari M. Turner, and Masaki Oshikawa. Entanglement spectrum of a topological phase in one dimension. *Physical Review B*, 81(6):064439, February 2010. arXiv: 0910.1811.
- [5] Steven R. White. Density matrix formulation for quantum renormalization groups. *Physical Review Letters*, 69(19):2863–2866, November 1992. Publisher: American Physical Society.
- [6] N. V. Prokof'ev, B. V. Svistunov, and I. S. Tupitsyn. Exact, complete, and universal continuous-time worldline Monte Carlo approach to the statistics of discrete quantum systems. *Journal of Experimental and Theoretical Physics*, 87(2):310–321, August 1998. Publisher: Pleiades Publishing Ltd.
- [7] Matthias Troyer and Uwe-Jens Wiese. Computational complexity and fundamental limitations to fermionic quantum Monte Carlo simulations. *Physical Review Letters*, 94(17):170201, May 2005. arXiv: cond-mat/0408370.
- [8] Frank Pollmann and Ari M. Turner. Detection of Symmetry Protected Topological Phases in 1D. *Physical Review B*, 86(12):125441, September 2012. arXiv: 1204.0704.
- [9] G. De Chiara, M. Lewenstein, and A. Sanpera. Bilinear-biquadratic spin-1 chain undergoing quadratic Zeeman effect. *Physical Review B*, 84(5), August 2011. Publisher: American Physical Society (APS).
- [10] R. Rossi, N. Prokof'ev, B. Svistunov, K. Van Houcke, and F. Werner. Polynomial complexity despite the fermionic sign. *EPL (Europhysics Letters)*, 118(1):10004, April 2017. arXiv: 1703.10141.

- [11] Ulrich Schollwöck. The density-matrix renormalization group in the age of matrix product states. *Annals of Physics*, 326(1):96–192, January 2011. Publisher: Elsevier BV.
- [12] David Ceperley. An Overview of Quantum Monte Carlo Methods. *Reviews in Mineralogy and Geochemistry - REV MINERAL GEOCHEM*, 71:129–135, 2010.
- [13] Robert D. Richtmyer, Stanis\law Ulam, and John von Neumann. Statistical methods in neutron diffusion. Technical Report LAMS-551, inst-LASL, inst-LASL:adr, April 1947.
- [14] Nicholas Metropolis and S. Ulam. The Monte Carlo Method. *Journal of the American Statistical Association*, 44(247):335–341, 1949. Publisher: [American Statistical Association, Taylor & Francis, Ltd.].
- [15] D.E. Knuth. *Art of Computer Programming, Volume 2: Seminumerical Algorithms*. Pearson Education, 2014.
- [16] N. Metropolis, A. W. Rosenbluth, M. Rosenbluth, A. H. Teller, and E. Teller. Equation of state calculations by fast computing machines. *Journal of Chemical Physics*, 21:1087–1092, 1953.
- [17] W. K. Hastings. Monte Carlo Sampling Methods Using Markov Chains and Their Applications. *Biometrika*, 57(1):97–109, 1970. Publisher: [Oxford University Press, Biometrika Trust].
- [18] Lars Onsager. Crystal Statistics. I. A Two-Dimensional Model with an Order-Disorder Transition. *Phys. Rev.*, 65(3-4):117–149, February 1944. Publisher: American Physical Society.
- [19] Lev Davidovich Landau. *On the theory of phase transitions. I.* 1937. Journal Abbreviation: Phys. Z. Sowjet.
- [20] Nikolay Prokof'ev and Boris Svistunov. Worm algorithms for classical statistical models. *Physical Review Letters*, 87(16):160601, September 2001. arXiv: cond-mat/0103146.
- [21] R. P. Feynman. Atomic Theory of the λ Transition in Helium. *Phys. Rev.*, 91(6):1291–1301, September 1953. Publisher: American Physical Society.
- [22] Hal Tasaki. *Physics and mathematics of quantum many-body systems*. Graduate texts in physics. Springer Nature, Cham, Switzerland, 2020.
- [23] Naoki Kawashima and Kenji Harada. Recent Developments of World-Line Monte Carlo Methods. *Journal of the Physical Society of Japan*, 73(6):1379–1414, June 2004. Publisher: Physical Society of Japan.
- [24] Henrik Bruus and Karsten Flensberg. *Many-body quantum theory in condensed matter physics: an introduction*. Oxford graduate texts. Oxford University Press, Oxford ; New York, 2004. OCLC: ocm56694794.

- [25] Markus Greiner, Olaf Mandel, Tilman Esslinger, Theodor W. Hänsch, and Immanuel Bloch. Quantum phase transition from a superfluid to a Mott insulator in a gas of ultracold atoms. *Nature*, 415(6867):39–44, January 2002.
- [26] Lode Pollet, Kris Van Houcke, and Stefan M.A. Rombouts. Engineering local optimality in quantum Monte Carlo algorithms. *Journal of Computational Physics*, 225(2):2249–2266, August 2007. Publisher: Elsevier BV.
- [27] Elliott Lieb, Theodore Schultz, and Daniel Mattis. Two soluble models of an antiferromagnetic chain. *Annals of Physics*, 16(3):407–466, December 1961.
- [28] N. Prokof'ev and B. Svistunov. Worm Algorithm for Problems of Quantum and Classical Statistics. *arXiv:0910.1393 [cond-mat, physics:hep-lat]*, May 2010. arXiv: 0910.1393.
- [29] Ribhu K. Kaul. Spin nematic ground state of the triangular lattice S=1 biquadratic model. *Physical Review B*, 86(10):104411, September 2012. arXiv: 1208.4133.
- [30] Kouichi Okunishi and Kenji Harada. Symmetry-protected topological order and negative-sign problem for $\mathrm{SO}(N)$ bilinear-biquadratic chains. *Physical Review B*, 89(13):134422, April 2014. Publisher: American Physical Society.
- [31] R. F. BISHOP and D. J. J. FARRELL. MARSHALL-PEIERLS SIGN RULES, THE QUANTUM MONTE CARLO METHOD, AND FRUSTRATION. *International Journal of Modern Physics B*, 15(10n11):1736–1739, 2001. _eprint: <https://doi.org/10.1142/S0217979201006264>.
- [32] H. Bethe. Zur Theorie der Metalle: I. Eigenwerte und Eigenfunktionen der linearen Atomkette. *Zeitschrift fuer Physik*, 71(3-4):205–226, March 1931.
- [33] F. D. M. Haldane. Continuum dynamics of the 1-D Heisenberg antiferromagnet: Identification with the O(3) nonlinear sigma model. *Physics Letters A*, 93(9):464–468, February 1983.
- [34] A. Einstein, B. Podolsky, and N. Rosen. Can Quantum-Mechanical Description of Physical Reality Be Considered Complete? *Physical Review*, 47:777–780, May 1935.
- [35] J. S. Bell. On the Einstein Podolsky Rosen paradox. *Physics Physique Fizika*, 1(3):195–200, November 1964. Publisher: American Physical Society.
- [36] Mark M. Wilde. *Quantum Information Theory*. Cambridge University Press, Cambridge, 2013.
- [37] Gilbert Strang. *Linear Algebra and Learning from Data*. Wellesley-Cambridge Press, January 2019. Google-Books-ID: L0Y_wQEACAAJ.
- [38] M. B. Hastings. An Area Law for One Dimensional Quantum Systems. *Journal of Statistical Mechanics: Theory and Experiment*, 2007(08):P08024–P08024, August 2007. arXiv: 0705.2024.

- [39] F. Verstraete, V. Murg, and J. I. Cirac. Matrix product states, projected entangled pair states, and variational renormalization group methods for quantum spin systems. *Advances in Physics*, 57(2):143–224, 2008. Publisher: Taylor & Francis _eprint: <https://doi.org/10.1080/14789940801912366>.
- [40] Zeph Landau, Umesh Vazirani, and Thomas Vidick. A polynomial-time algorithm for the ground state of 1D gapped local Hamiltonians. *arXiv:1307.5143 [cond-mat, physics:quant-ph]*, July 2013. arXiv: 1307.5143.
- [41] G. Vidal, J. I. Latorre, E. Rico, and A. Kitaev. Entanglement in quantum critical phenomena. *Physical Review Letters*, 90(22):227902, June 2003. arXiv: quant-ph/0211074.
- [42] Marcel den Nijs and Koos Rommelse. Preroughening transitions in crystal surfaces and valence-bond phases in quantum spin chains. *Physical Review B*, 40(7):4709–4734, September 1989. Publisher: American Physical Society.
- [43] Ian Affleck, Tom Kennedy, Elliott H. Lieb, and Hal Tasaki. Rigorous results on valence-bond ground states in antiferromagnets. *Physical Review Letters*, 59:799–802, August 1987. ADS Bibcode: 1987PhRvL..59..799A.
- [44] G. De Chiara, M. Lewenstein, and A. Sanpera. Bilinear-biquadratic spin-1 chain undergoing quadratic Zeeman effect. *Physical Review B*, 84(5), August 2011.
- [45] Tom Kennedy and Hal Tasaki. Hidden symmetry breaking and the Haldane phase in $S=1$ quantum spin chains. *Communications in Mathematical Physics*, 147(3):431–484, January 1992. Publisher: Springer.
- [46] Ian Affleck, Tom Kennedy, Elliott H. Lieb, and Hal Tasaki. Rigorous results on valence-bond ground states in antiferromagnets. *Physical Review Letters*, 59:799–802, August 1987.
- [47] Dominik Hangleiter, Ingo Roth, Daniel Nagaj, and Jens Eisert. Easing the Monte Carlo sign problem. *Science Advances*, 6(33):eabb8341, August 2020. arXiv: 1906.02309.

Selbständigkeitserklärung

Ich versichere hiermit, die vorliegende Arbeit mit dem Titel

**Untersuchung des bilinearen-biquadratischen Spin-1 Modells mithilfe
der Quanten-Monte-Carlo-Methode**

selbständig verfasst zu haben und keine anderen als die angegebenen Quellen und
Hilfsmittel verwendet zu haben.

Julian Durnwalder

München, den 21. Jannuar 2022